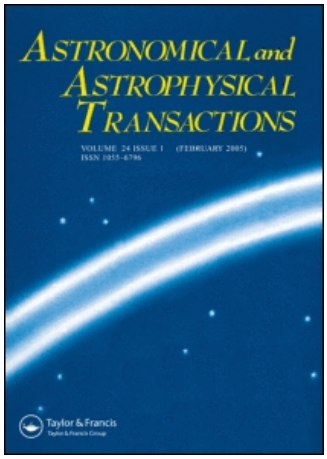

Astronomical & Astrophysical Transactions
The Journal of the Eurasian Astronomical Society
Publication details, including instructions for authors and subscription information:
http://www.informaworld.com/smpp/title~content=t713453505

On broad emission-line profiles from active galactic nuclei

R. Wayte

Online Publication Date: 01 February 2004
To cite this Article: Wayte, R. (2004) 'On broad emission-line profiles from active galactic nuclei', Astronomical & Astrophysical Transactions, 23:1, 1 - 33
To link to this article: DOI: 10.1080/10556790310011118
URL: http://dx.doi.org/10.1080/10556790310011118

Astronomical and Astrophysical Transactions
Vol. 23, No. 1, February 2004, pp. 1–33

ON BROAD EMISSION-LINE PROFILES FROM ACTIVE GALACTIC NUCLEI

R. WAYTE*

29 Audley Way, Ascot, Berkshire SL5 8EE, UK

(Received 25 February 2003)

A broad-line region (BLR) disc model is derived and fitted to 121 published broad emission-line profiles from quasistellar objects (QSOs) and Seyfert I galaxies. Keplerian rotation of material in calm circular orbits, plus stimulated non-isotropic emission is best suited to explain the observed profiles. BLR discs in QSOs are, within the framework of the model, found to be tapered and extensive, whereas Seyfert I discs are usually fanned out but equally extensive. The material density in each disc appears to be constant with radius. In QSO emission-line profiles, the peak relative to adjacent continuum intensity increases with increasing logarithm of disc mass or maximum radius, on average.

Keywords: Quasistellar objects; Emission lines; Seyfert I galaxies

1 INTRODUCTION

A complete model is still required for the broad-line region of active galactic nuclei (AGNs) (Osterbrock, 1989, 1991). Dumont *et al.* (1998) have stated that some fundamental key is missing in our understanding of AGNs.

The most common inferred properties of the broad emission-line regions are that the material velocity must increase inwards, with electron density and ionization parameter. A rotational velocity field about a central body is favoured, on the basis of AGN accretion disc model. Neither radial infall nor outflow of material is indicated by reverberation mapping techniques of Seyfert I galaxies. Van Groningen (1983) has produced reasonable line profiles from a turbulent rotating-disc model with weak axial jets or radial winds. Symmetric line profiles from publications form the basis of the broad-line region (BLR) model presented here.

2 THEORETICAL BROAD-LINE PROFILES

The broad-line profiles of quasistellar objects (QSOs) are remarkably similar, implying that few physical variables are involved in their production. Around half are symmetric; so the fundamental profile-generating mechanism must be symmetric. Any asymmetry is then

* E-mail: rwayte@audsci.fsnet.co.uk

ISSN 1055-6796 print; ISSN 1476-3540 online
DOI: 10.1080/10556790310011118

due to the addition of flux as caused by bipolar axial flow for example, or subtraction of flux as caused by absorption or reduced emission in certain disc areas.

Consider a thin axisymmetric annulus of isotropically emitting material, orbiting around a central mass M at constant velocity v (Fig. 1(a)). Let the observer view the annulus edge on such that an elemental mass at P has a velocity component

$$u = v\cos\varphi, \tag{1}$$

away from the observer. This element and its corresponding partner at Q will produce the total line profile intensity found at a red-shifted wavelength position $\lambda \approx \lambda_0(1+u/c)$, where λ_0 is the line profile centre wavelength for the whole annulus. For $\varphi = \omega t$, differentiation of Eq. (1) and rearrangement yield

$$\delta t \approx \frac{\delta u}{\omega(v^2 - u^2)^{1/2}}. \tag{2}$$

Now, the velocity element δu corresponds to the profile wavelength interval $\delta\lambda \approx (\delta u/c)\lambda_0$ at wavelength λ. So δt is the time interval during which material elements at P and Q contribute to the line profile interval $\delta\lambda$ at λ. Consequently, the line profile intensity I_{au} is proportional to δt or the material in the angular element $\delta\varphi = \omega\ \delta t$ located at angle φ:

$$I_{\text{au}} \approx \text{constant} \times \frac{\delta u}{(v^2 - u^2)^{1/2}}, \tag{3a}$$

$$\approx \text{constant} \times \frac{\delta\lambda}{[(\lambda_{\max} - \lambda_0)^2 - (\lambda - \lambda_0)^2]^{1/2}}. \tag{3b}$$

This line profile is illustrated in Figure 1(b) and is unlike any observed profile. However, by integrating over a disc with selected density, extent and excitation, some apparently natural profiles may be calculated.

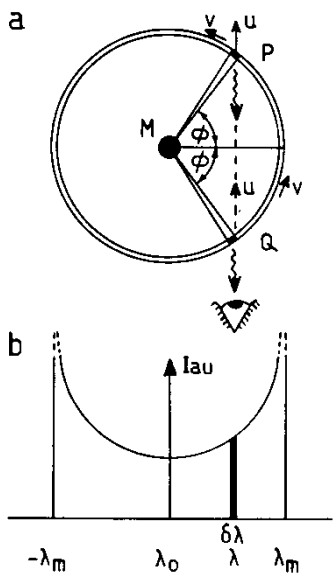

FIGURE 1 (a) Schematic diagram for an annulus of light-emitting material rotating at a velocity v around a mass M. (b) Spectrum produced by this annulus for emission at the rest wavelength λ_0.

In all these calculations the velocities should be understood as neglecting the unknown angle of view between the observer and the rotating-disc axis. For random orientations, actual disc velocities are on average 32% higher than observed velocities.

3 BROAD-LINE PROFILES IN QUASISTELLAR OBJECTS

3.1 Development of a Model

We shall start by selecting disc parameters which yield theoretical line profiles such as the simplest profiles from QSOs. Two distinct disc models can account for the profiles, by suitable choice of excitation method, as follows.

3.1.1 Excitation Through the Disc Itself

Figure 2(a) shows a schematic cross-section of a proposed accretion disc extending from radius r_1 to r_2, rotating around a compact massive source M of ionizing radiation. The effective disc thickness decreases with radius as $z \propto r^{-1/2}$. The material's local volume density ρ_v will be taken as constant (see Osterbrock, 1989, p. 367). Consequently, the line-emitting material in any annulus of incremental extent δr has mass $\delta m = \rho_v z 2\pi r\, \delta r$. If F_0 is the total flux from M then, for negligible absorption, the excitation at S would be determined by geometry as

$$\delta f \propto F_0 \frac{2\pi r z}{4\pi r^2} \rho_v\, \delta r = F_0 \frac{k_z}{2r^{3/2}} \rho_v\, \delta r, \tag{4a}$$

where k_z is constant. If the local disc thickness were changed arbitrarily to $z =$ constant or $z \propto r^{-1}$, the profile fits would be poor unless the density ρ_v were changed to compensate.

3.1.2 Excitation of the Disc Surface From Above

Consider the situation in which the disc is rotating around a central bulge or torus of hot material, which acts as the source of exciting radiation. Each element of this source above

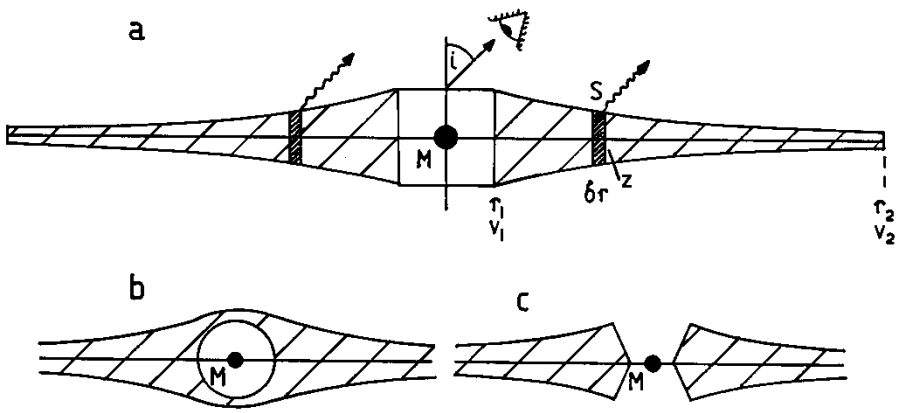

FIGURE 2 (a) Schematic cross-section of the BLR disc rotating around the central radiation source M. A typical element annulus at S is shown, of width δr and breadth z. (b) A BLR disc similar to (a) but with a central bulge as proposed for radio-quiet QSOs. (c) A BLR disc in which the centre material has been blown back to expose the source, as proposed for radio-loud QSOs.

the disc plane may illuminate the disc surface obliquely. If the disc is optically thin, when viewed from above, then equation (4a) still applies. However, for an optically thick disc, δf would vary as r^{-2} rather than as $r^{-3/2}$, which does not fit the observed profiles very well. Therefore we shall continue on the assumption that the disc is optically thin whether illuminated from a central point or a bulge or torus.

Thus, for the complete disc, Eqs. (3) and (4a) will be used to describe the radiation from every incremental annulus, of constant mass density, due to a central source of energy. However, to secure good agreement with spectra we shall postulate that emission from this material involves light amplification by stimulated emission of radiation, with preferred direction of emission. This radical step has been taken because more prosaic processes have failed. Necessary conditions for our model are therefore that the accretion disc must be calm with circular material orbits and little turbulence, for good velocity coherence. In addition, the emitting atoms are aligned with their axes of angular momentum parallel to the orbits. This is in agreement with the observation of apparent toroidal fields in galactic material (Haas *et al.*, 1998; Beck, 1982). Consequently, the aligned electrons in atomic orbits act like loop aerials and emit line photons in preferred directions (Glazier and Lamont, 1958, p. 267). We observe this as an angle-dependent intensity variation such that material at P and Q in Figure 1 emits towards us with intensity $I = I_0 \sin^2 \varphi$. This is very effective at removing the twin spectral peaks, since $I = \varphi = 0$ when $u = v$. Each emitted line photon may also stimulate other excited atoms into emitting line photons (see Appendix A). The amount of stimulated emission is much greater than for normal negative absorption because of the controlled alignment of atoms. So the final emission in our direction becomes

$$E = E_0 \exp(e \sin^2 \varphi). \tag{4b}$$

Equations (3a), (4a) and (4b) may now he combined and integrated over every incremental annulus in the disc. Absorption of incident radiation from M will not be included explicitly at this stage. Thus, the final line-profile intensity as a function of u/v_1 is

$$I_{\mathrm{d}u} = \text{constant} \times \delta u \int_{v=v_2}^{v=v_1} (v^2 - u^2)^{-1/2} \exp(e \sin^2 \varphi) r^{-3/2} \, \mathrm{d}r. \tag{5a}$$

For circular Keplerian orbits with $GM = v^2 r$, and $u = v \cos \varphi$, then

$$I_{\mathrm{d}u} = \text{constant} \times \int_{\varphi_2}^{\varphi_1} \exp(e \sin^2 \varphi) \frac{\mathrm{d}\varphi}{\cos \varphi}, \tag{5b}$$

where $\varphi_1 = \arccos(u/v_1)$ and $\varphi_2 = \arccos(u/v_2)$ when $u < v_2$ or $\varphi_2 = 0$ for $u \geq v_2$.

Figure 3 illustrates the calculated line profile intensity $I_{\mathrm{d}u}$ (arbitrary units) as a function of the velocity parameter u/v_1 for a number of chosen disc cut-off velocities v_2/v_1. (Recall that $u/v_1 = (\lambda - \lambda_0)/(\lambda_{\max} - \lambda_0)$.) The upper curve is universal as far as each break point v_2/v_1; so profiles from different discs have this high-velocity wing in common. This agrees with the noted similarities in observed profiles. A profile becomes more peaked as each outer annulus is added. When fitting to real profiles, amplitude scaling has to be adjusted, as does the continuum level to fix the $u/v_1 = 1$ point at the full-width zero-intensity value.

Good fits to 52 published QSO profiles are illustrated in Figure 4, and their model characteristic parameters given in Table I. This collection of differently shaped profiles and disc sizes justify the great effort expended by astronomers on recording high-quality spectra. Table I shows that all the BLR discs are greater in extent than $r_2/r_1 = 10$ and a few are extremely extensive up to $r_2/r_1 = 2500$. Different ion species occupy only limited parts of the complete BLR disc according to their v_1 and v_2 values. It is remarkable that this set of 52 profiles requires only one variable v_2/v_1, plus scaling.

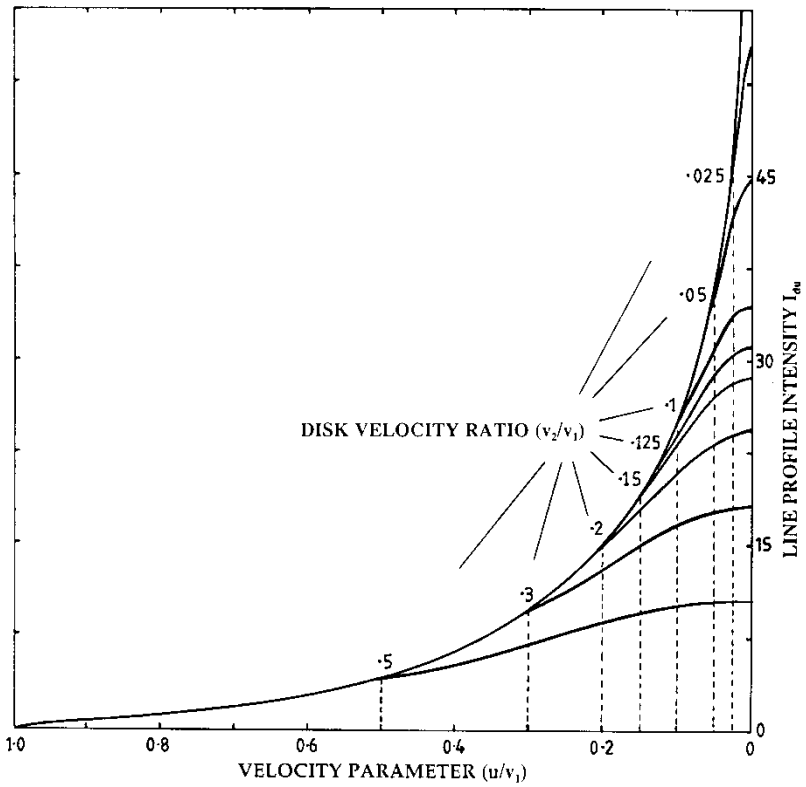

FIGURE 3 The calculated line profile intensity I_{du}, as a function of the velocity parameter u/v_1 for various disc velocity ratios v_2/v_1.

One interesting aspect of this model concerns the total observed flux I_T contained within an emission-line profile. Upon integrating equation (5a) with respect to u (while keeping r and v constant), and then integrating for r, we obtain

$$I_T = \text{constant} \times (r_1^{-1/2} - r_2^{-1/2}) = \text{constant} \times v_1\left(1 - \frac{v_2}{v_1}\right). \tag{6}$$

Evidently, the far reaches of extensive discs add little flux to the profile but influence the full width at half-maximum (FWHM) value significantly. For example, the average QSO in Table I has $v_2/v_1 \approx 0.125$; so $I_{T(\text{average})} = \text{constant} \times 0.875$. Half this flux comes from the inner disc up to $v/v_1 \approx 0.56$, or $r/r_1 \approx 3.2$. That is, 0.25% of the total disc area, which is nearest to the source of excitation, contributes as much flux to the emission-line profile as the remaining 99.75%.

A plot (not illustrated here) of v_1/v_2 versus v_1 for QSOs in Table I has revealed that there is a general increase in disc size r_2/r_1 with increasing v_1. The scattered data exhibited a rough average of $v_1/v_2 \approx 10$ for $v_1 \approx 11\,000$ km s^{-1}. Evidently, the more massive sources can support and illuminate larger discs. Given the disc properties used in equation (4a), then the disc mass increases with increasing radius as

$$M_d = \int_{r_1}^{r_2} \rho_v z 2\pi r \, dr = \rho_v k_z \frac{4\pi}{3}(r_2^{3/2} - r_1^{3/2}). \tag{7}$$

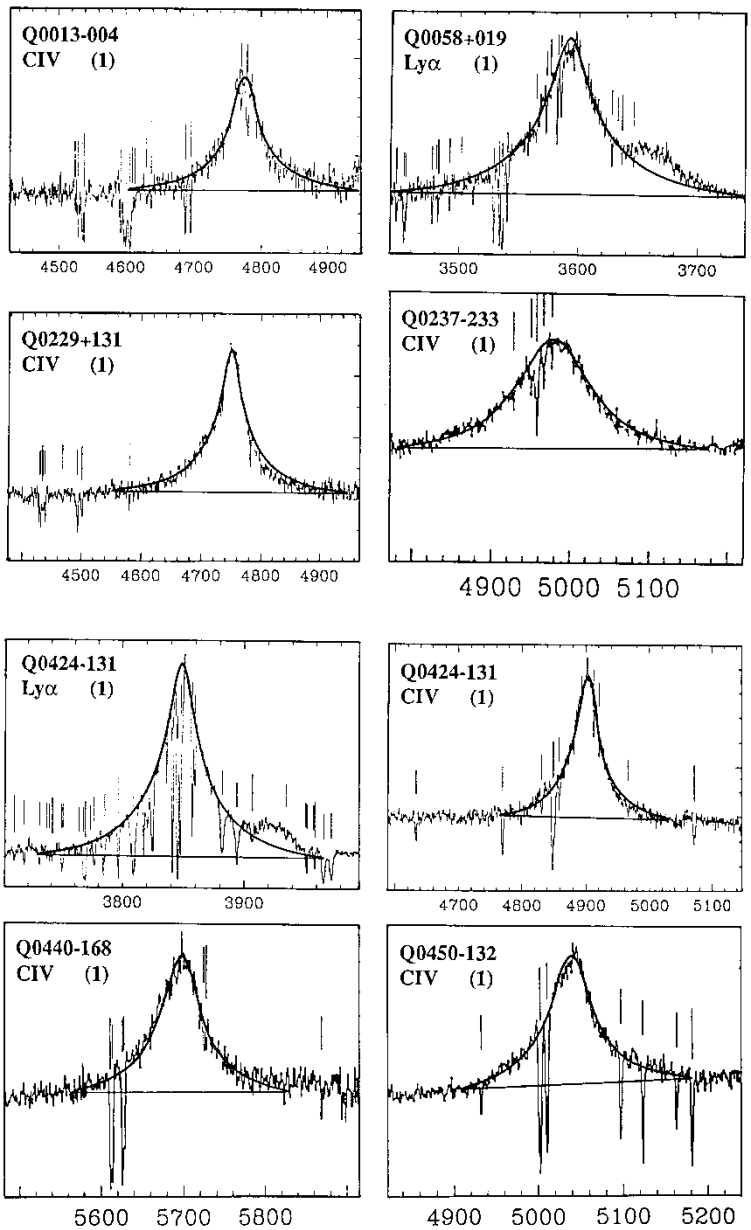

FIGURE 4 (a)–(g) Calculated QSO emission-line profiles fitted to various observed profiles taken from the literature, as listed in Table I, where the relevant references will be found. The way in which our single profile fits the composite C III and Mg II examples better than the two superimposed Gaussian profiles published is shown in (g).

Let us briefly reconsider the disc parameters which led to these theoretical profiles, namely $z = k_z/r^{1/2}$ and ρ_v constant. Figure 2(a) shows an ideal disc cross-section schematic diagram, but in practice the inner disc region may look like Figure 2(b) for radio-quiet QSOs, or like Figure 2(c) for radio-loud QSOs where the inner disc material has been blown back. Consequently, the continuum photo-ionization source may be more directly visible in radio-loud QSOs. Brotherton *et al.* (1994) found that radio-quiet QSOs have broader C IV

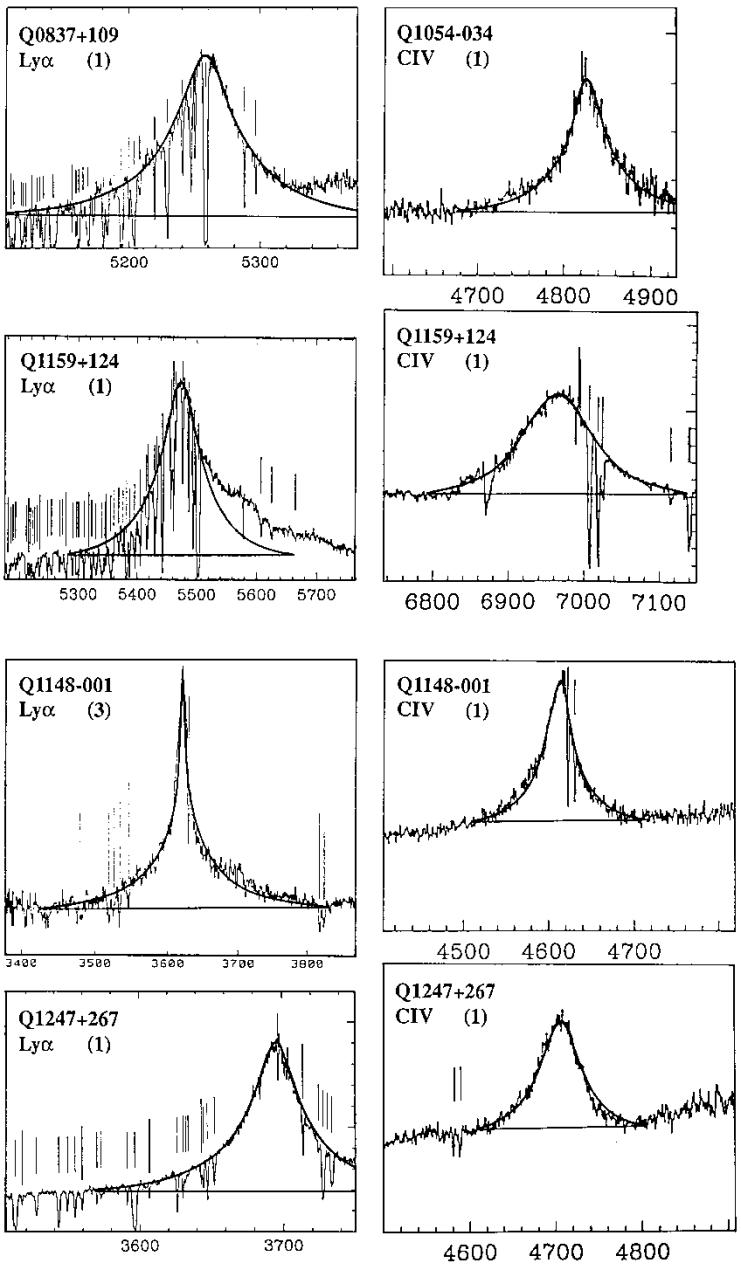

FIGURE 4b (*Continued*)

($\lambda = 1549$ Å) lines than radio-loud objects, but the Mg II FWHMs do not differ. The C IV region in radio-quiet objects is therefore nearer the source, probably.

3.2 Application of Model to Some Published Profile Analyses

We shall now see how well our single-component disc model fits some published QSO analyses. Figure 3 may be measured directly to obtain an empirical relationship for peak

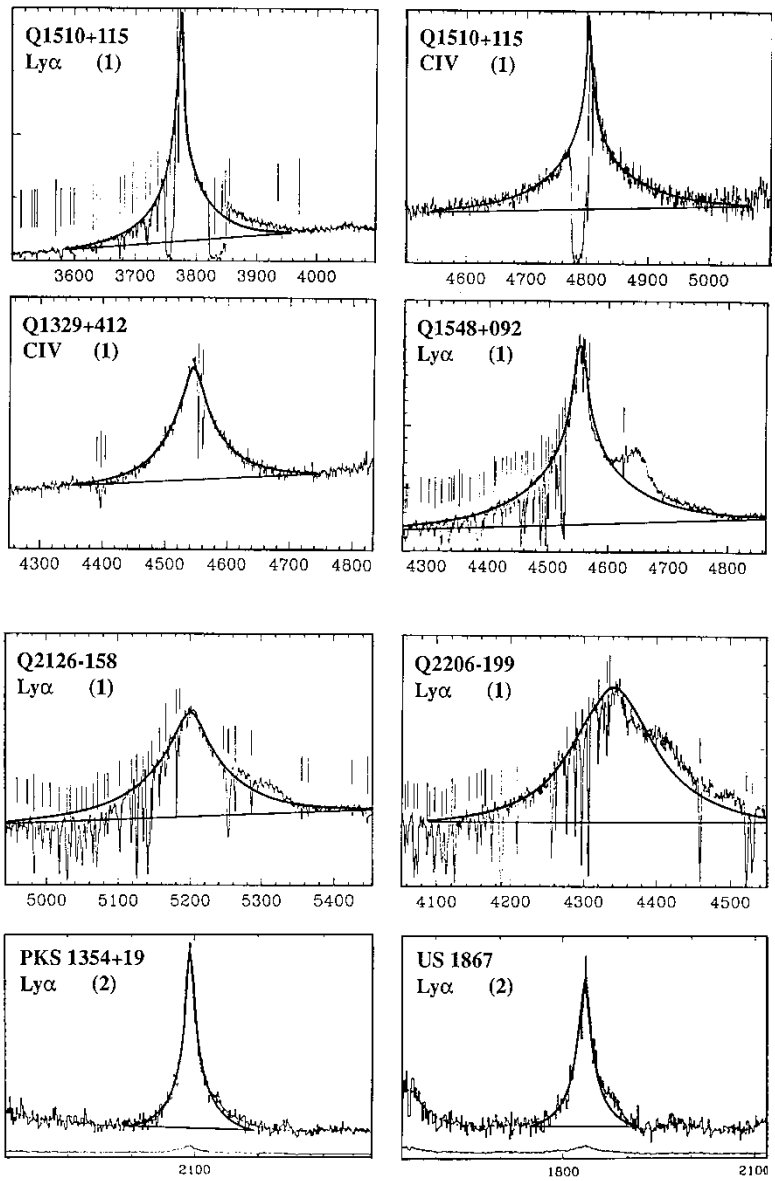

FIGURE 4c (*Continued*)

intensity I_p, the half-width at half-maximum (HWHM) velocity u_{HWHM}/v_1 and the disc cut-off velocity v_2/v_1:

$$I_p \approx 0.9\left[\ln\left(\frac{v_1}{u_{HWHM}}\right)^2 - 1\right]\exp(e) \approx \ln\left(\frac{v_1}{v_2}\right)\exp(e). \tag{8a}$$

The HWHM velocity value decreases as $(v_2/v_1)^{5/9}$, while the profile peak value increases as $\ln(v_1/v_2)$.

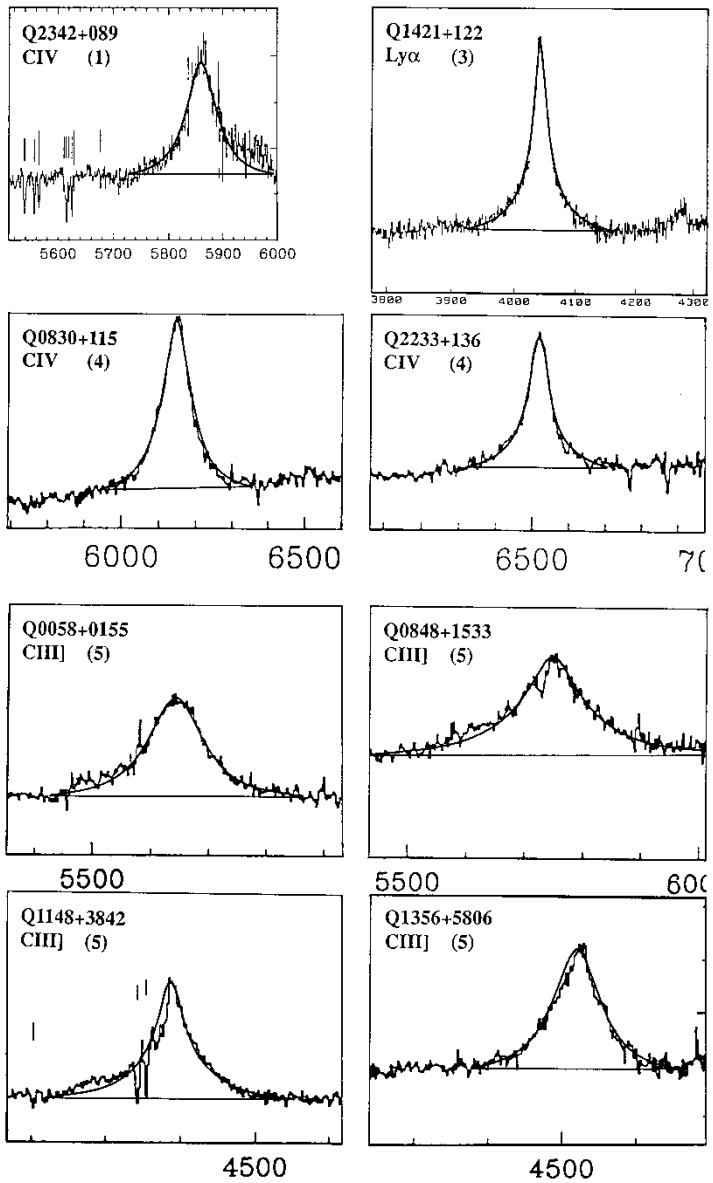

FIGURE 4d (*Continued*)

In order to grasp the real magnitude of the extreme velocities found in BLR discs, a number of C IV emission-line profiles from the work of Sargent *et al.* (1988) have been measured for their HWHM equivalent disc rotation velocities. Figure 5 illustrates these velocities relative to the velocity of light, plotted as C/V for easier comprehension.

To compare equation (8a) with observed data, it is necessary to introduce an appropriate continuum intensity I_c. For example, as drawn on the data replotted from the work of Wills *et al.* (1993), Figure 6 shows a straight line for

$$\frac{I_p}{I_c} \approx -1.30 \ln [\text{FWHM}(\text{km s}^{-1})] + 12.05. \tag{8b}$$

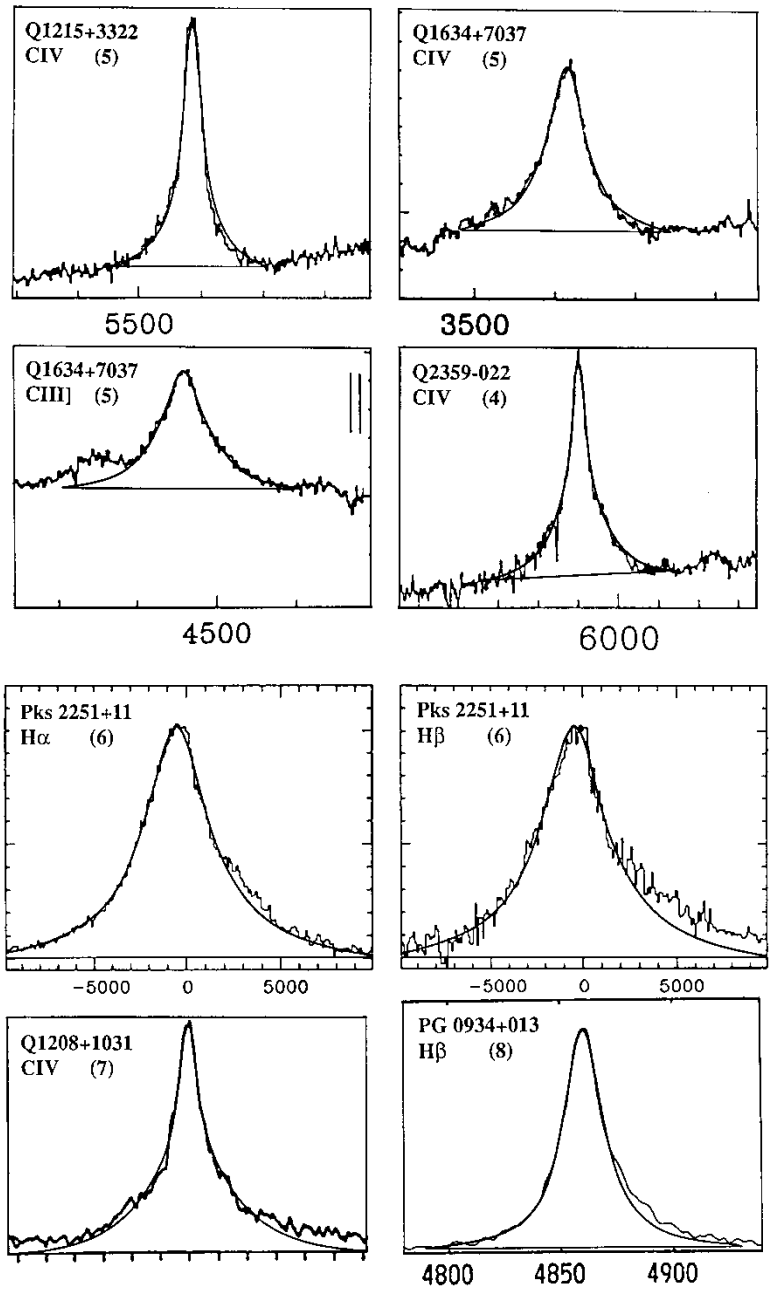

FIGURE 4e (*Continued*)

A central value ($I_p/I_c = 1.15$) has been delineated for a FWHM of 4380 km s^{-1}, corresponding to the mean HWHM equivalent disc rotation velocity in Figure 5. Now given that $GM = v^2 r$ in the disc, the HWHM radius r_{hw} may be substituted in equation (8b) to obtain

$$\frac{I_p}{I_c} \approx 0.65 \ln(\text{constant} \times r_{hw}). \tag{8c}$$

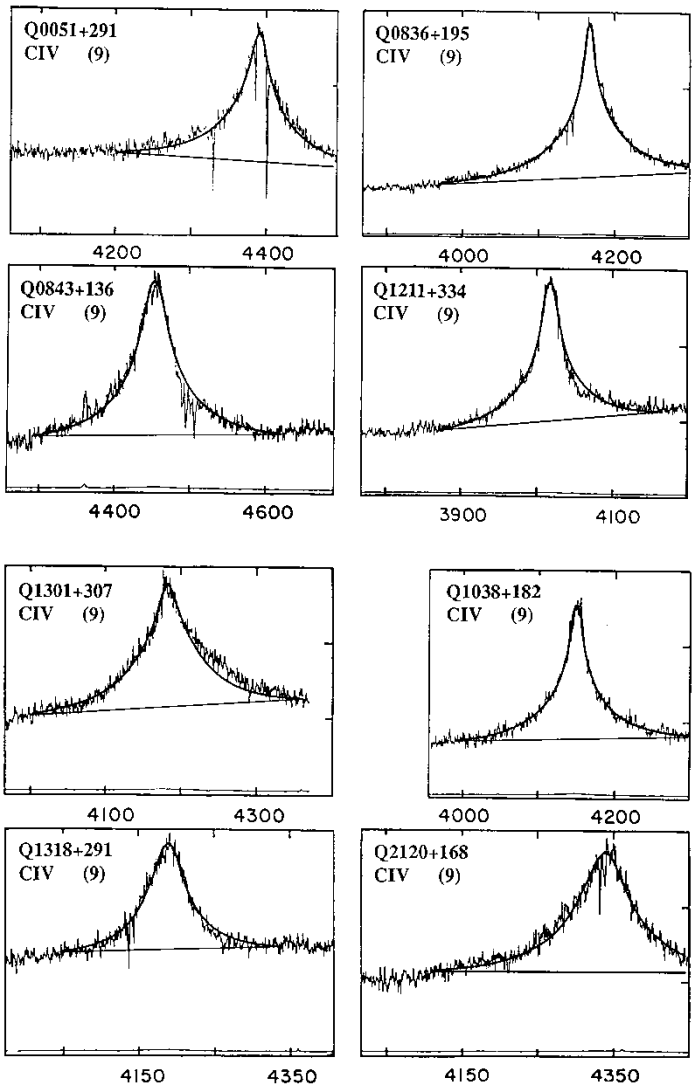

FIGURE 4f (*Continued*)

Thus, there is on average a logarithmic increase in profile relative peak intensity with increasing disc radius. This agrees with equation (8a) for an averaged I_c and v_1. Alternatively, we could use Eq. (7) for the disc mass and write

$$\frac{I_p}{I_c} \propto \ln(\text{constant} \times M_d). \tag{8d}$$

A line-shape parameter, used by Wills *et al.* (1993), is defined in terms of full width at one-quarter maximum intensity (FW($\frac{1}{4}$)M) and full width at three-quarters maximum intensity (FW($\frac{3}{4}$)M):

$$S = \frac{\text{FW}(\frac{1}{4})\text{M} - \text{FW}(\frac{3}{4})\text{M}}{\text{FWHM}}. \tag{8e}$$

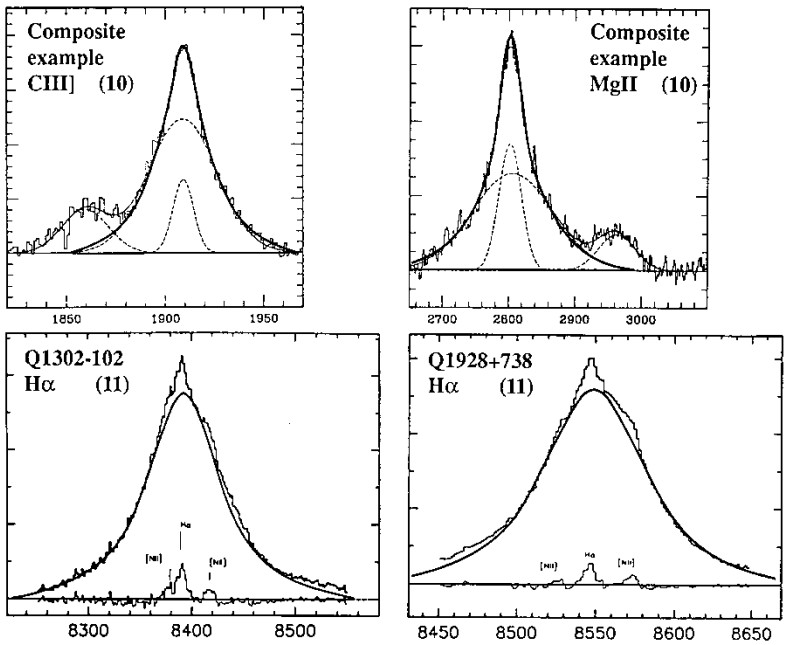

FIGURE 4g (*Continued*)

By measuring Figure 3 directly again, we can derive an empirical law for S as

$$\ln S \approx -0.65 \ln [\text{FWHM}(\text{km s}^{-1})] + 5.69. \tag{8f}$$

This equation has been applied to the log[S(C IV)] versus log[FWHM(C IV)] plot by Wills *et al.* (1993), and it fits the scattered data very well. The most common value of S for QSOs there is 1.3, which corresponds to our $v_2/v_1 \approx 0.125$) in Table I.

Theoretical profiles in Figure 3 also obey the formula

$$e(\ln S) \approx \ln\left(\frac{v_1}{4v_2}\right), \tag{8g}$$

within 5% for $1 < S < 1.75$, which would cover most real profiles. If the measured value of v_1 is uncertain, then v_2/v_1 derived from equations (8e) and (8g) may be introduced into equation (8a) to obtain a more accurate v_1.

A few of the inferences mentioned by other investigators are satisfied by our model. For example, Dumont *et al.* (1998) interpreted line profiles for a photo-ionization accretion disc model. Definite ionization fronts occurred for different species as a function of distance from the source. Line ratios were not those expected for normal spontaneous emission. Penston *et al.* (1990b) have suggested the possibility of anisotropic continuum emission. Baldwin *et al.* (1995) calculated that selection effects dominate efficient BLR line emission. In general, published BLR disc models try to fill the gap between the twin peaks of a profile, whereas our model attenuates the peaks by using equation (4b).

TABLE I QSO Broad Emission-Lines.

Object	*Ion*	*z*	*FWHM (km s^{-1})*	*v_1 (km s^{-1})*	*v_2 (km s^{-1})*	*r_2/r_1*	*Reference*	*Figure*
Q0013-004	C IV	2.083	3410	10 670	1065	100	Sargent *et al.* (1988)	4(a)
Q0058 + 019	Lyα	1.959	4230	11 750	1175	100	Sargent *et al.* (1988)	4(a)
Q0229 + 131	C IV	2.068	3840	15 360	1135	183	Sargent *et al.* (1988)	4(a)
Q0237-233	C IV	2.219	6770	12 030	3010	16	Sargent *et al.* (1988)	4(a)
Q0424-131	Lyα	2.167	3115	9350	805	135	Sargent *et al.* (1988)	4(a)
Q0424-131	C IV	2.164	2850	8250	825	100	Sargent *et al.* (1988)	4(a)
Q0440-168	C IV	2.678	3110	7000	1050	44	Sargent *et al.* (1988)	4(a)
Q0450-132	C IV	2.255	3545	7680	1150	44	Sargent *et al.* (1988)	4(a)
Q0837 + 109	Lyα	3.323	3320	8820	1105	64	Sargent *et al.* (1988)	4(b)
Q1054-034	C IV	2.111	3115	9520	950	100	Sargent *et al.* (1988)	4(b)
Q1159 + 124	Lyα	3.505	4820	10 955	1480	55	Sargent *et al.* (1988)	4(b)
Q1159 + 124	C IV	3.500	4855	7630	2290	11.1	Sargent *et al.* (1988)	4(b)
Q1148-001	Lyα	1.979	1480	16 850	335	2500	Young *et al.* (1982)	4(b)
Q1148-001	C IV	1.980	2490	6635	830	64	Sargent *et al.* (1988)	4(b)
Q1247 + 267	Lyα	2.041	3515	10 300	1030	100	Sargent *et al.* (1988)	4(b)
Q1247 + 267	C IV	2.036	3550	6210	1550	16	Sargent *et al.* (1988)	4(b)
Q1510 + 115	Lyα	2.106	1750	14 300	285	2500	Sargent *et al.* (1988)	4(c)
Q1510 + 115	C IV	2.102	1965	16 580	330	2500	Sargent *et al.* (1988)	4(c)
Q1329 + 412	C IV	1.932	4755	10 570	1055	100	Sargent *et al.* (1988)	4(c)
Q1548 + 092	Lyα	2.750	3840	23 300	815	816	Sargent *et al.* (1988)	4(c)
Q2126-158	Lyα	3.280	5270	14 900	1490	100	Sargent *et al.* (1988)	4(c)
Q2206-199	Lyα	2.575	8660	17 550	3510	25	Sargent *et al.* (1988)	4(c)
PKS 1354 + 19	Lyα	0.720	3440	10 000	500	400	Bahcall *et al.* (1993)	4(c)
US 1867	Lyα	0.513	4560	13 500	1350	100	Bahcall *et al.* (1993)	4(c)
Q2342 + 089	C IV	2.782	3305	6825	1365	25	Sargent *et al.* (1988)	4(d)
Q1421 + 122	Lyα	—	2115	8800	440	400	Young *et al.* (1982)	4(d)

TABLE I (*Continued*).

Object	*Ion*	*z*	*FWHM (km s^{-1})*	*v_1 (km s^{-1})*	*v_2 (km s^{-1})*	*r_2/r_1*	*Reference*	*Figure*
Q0830 + 115	C IV	2.974	4215	9790	1665	35	Sargent *et al.* (1989)	4(d)
Q2233 + 136	C IV	3.211	3225	8560	1070	64	Sargent *et al.* (1989)	4(d)
Q0058 + 0155	C III	1.959	5600	11 400	2280	25	Steidel and Sargent (1992)	4(d)
Q0848 + 1533	C III	2.009	6320	16 600	2075	64	Steidel and Sargent (1992)	4(d)
Q1148 + 3842	C III	1.303	3930	11 800	1180	100	Steidel and Sargent (1992)	4(d)
Q1356 + 5806	C III	1.371	4880	9355	2105	20	Steidel and Sargent (1992)	4(d)
Q1215 + 3322	C IV	2.606	2100	6300	630	100	Steidel and Sargent (1992)	4(e)
Q1634 + 7037	C IV	1.334	4650	10 800	1620	44	Steidel and Sargent (1992)	4(e)
Q1634 + 7037	C III	1.334	4200	10 040	1505	44	Steidel and Sargent (1992)	4(e)
Q2359-022	C IV	2.814	3100	10 860	815	178	Sargent *et al.* (1989)	4(e)
PKS 2251 + 11	Hα	—	4285	10 720	1340	64	Stirpe (1990)	4(e)
PKS 2251 + 11	Hβ	—	4285	10 720	1340	64	Stirpe (1990)	4(e)
Q1208 + 1031	C IV	2.326	2665	12 000	600	400	Baldwin *et al.* (1988)	4(e)
PG 0934 + 013	Hβ	—	1340	4360	675	42	Corbin (1995)	4(e)
Q0051 + 291	C IV	1.832	3565	12 465	935	178	Foltz *et al.* (1986)	4(f)
Q0836 + 195	C IV	1.689	2630	14 600	365	1600	Foltz *et al.* (1986)	4(f)
Q0843 + 136	C IV	1.875	3795	11 400	1140	100	Foltz *et al.* (1986)	4(f)
Q1211 + 334	C IV	1.593	3110	10 865	815	178	Foltz *et al.* (1986)	4(f)
Q1301 + 307	C IV	1.700	5090	13 900	1390	100	Foltz *et al.* (1986)	4(f)
Q1308 + 182	C IV	1.677	2565	11 500	575	400	Foltz *et al.* (1986)	4(f)
Q1318 + 291	C IV	1.705	4335	10 310	1545	44	Foltz *et al.* (1986)	4(f)
Q2120 + 168	C IV	1.800	5915	15 480	1935	64	Foltz *et al.* (1986)	4(f)
Composite	C III	—	4105	9765	1465	44	Steidel and Sargent (1991)	4(g)
Composite	Mg II	—	6400	20 400	2040	100	Steidel and Sargent (1991)	4(g)
Q1302-102	Hα	0.286	2960	5925	1185	25	Jackson and Eracleous (1995)	4(g)
Q1928 + 738	Hα	0.302	2710	5420	1220	20	Jackson and Eracleous (1995)	4(g)

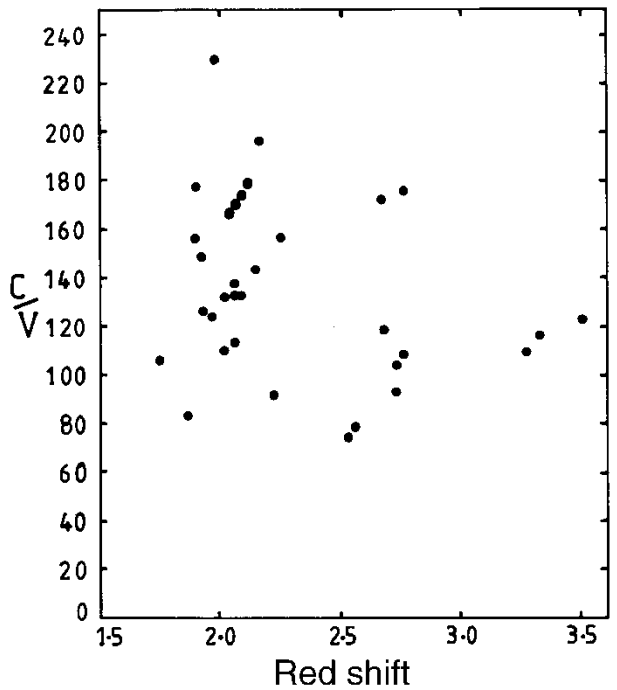

FIGURE 5 Half-width equivalent velocity relative to the velocity of light as a function of red shift for C IV emission-line profiles in some QSOs observed by Sargent *et al.* (1988).

3.3 Application to the Baldwin Effect

Another aspect shown by Wills *et al.* (1993) is that ln [EW(C IV)] decreases roughly with increase in ln [FWHM(C IV)]. This is probably connected with the so-called Baldwin effect which states that emission-line equivalent widths decrease generally as the continuum luminosity increases. Let I_T in Eq. (6) represent the emission-line luminosity L, and I_c be the continuum luminosity L_c. Then Eq. (6) becomes

$$L = \text{constant} \times L_c r_1^{-1/2}\left(1 - \frac{v_2}{v_1}\right), \tag{8h}$$

given that BLR disc illumination is expected to increase linearly with increasing central source and continuum luminosities. According to this equation, variation in $v_2/v_1 = (r_1/r_2)^{1/2}$ between 0.4 and 0.07 typically will add some scatter to L, but r_1 by itself may account for the Baldwin effect by increasing as L_c increases. (Remember that r_1 and r_2 are ionization front positions and not necessarily disc boundaries.) For example, Mg II ($\lambda = 2800$ Å) is thought to have an inner ionization front at a radius which increases with increasing central source luminosity. Conversely, C IV ($\lambda = 1549$ Å) is active much nearer the source and may sometimes have no inner ionization front other than the disc inner boundary. So r_1 for Mg II is going to vary with L_c from disc to disc more than r_1 for C IV.

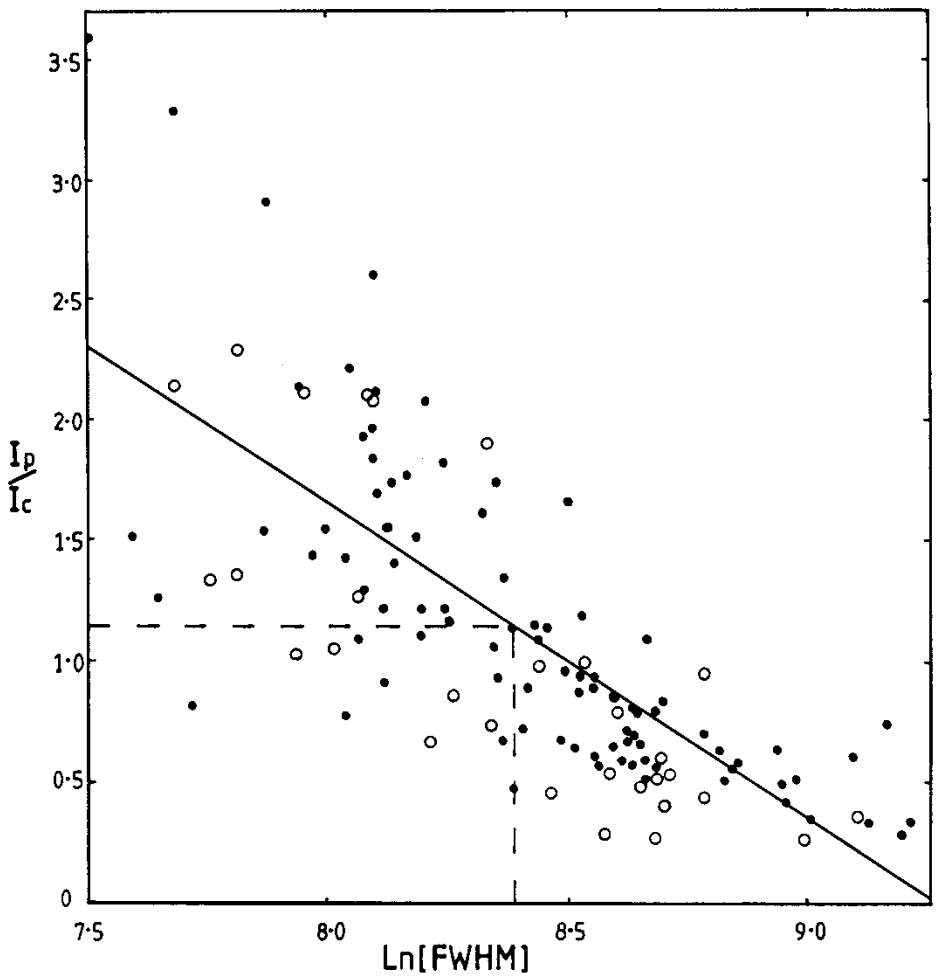

FIGURE 6 Emission-line peak intensity relative to the adjacent continuum intensity as a function of FWHM for C IV in QSOs studied by Wills *et al.* (1993): ——, approximate fit to the data such that $I_p/I_c = 1.15$ when the mean HWHM velocity is 2190 km s^{-1} in Figure 5; ○, radio-loud quasars; •, radio-quiet QSOs.

If the ionization front positions r_1 and r_2 for any particular ion are governed by incident flux density, then, according to equation (4a), $F_0/4\pi r_1^2$ should be a constant k_1 and $F_0/4\pi r_2^2$ another constant k_2. Thus, on the assumption that L_c is proportional to F_0, equation (8h) becomes

$$L = \text{constant} \times L_c L_c^{-1/4}\left[1 - \left(\frac{k_2}{k_1}\right)^{1/4}\right]; \tag{8i}$$

so $L \propto L_c^{3/4}$ and EW $\propto L_c^{-1/4}$. A stronger effect could be produced if saturation sets in so that the emission-line flux L cannot increase linearly with increasing F_0 or L_c. In addition, quasars of larger mass M (with higher luminosity generally) probably tend to have larger r_1 values, keeping v_1 near the normal range. A weaker effect would occur in QSOs where r_1 represents the BLR disc inner boundary rather than an ionization front and does not necessarily increase with increasing F_0 or M.

Baldwin (1977) and Baldwin *et al.* (1978) discovered that, for some types of quasar, EW(C IV) $\propto L_c^{-2/3}$. Kinney *et al.* (1990) have measured other quasars to obtain EW(C IV) $\propto L_c^{-0.17}$. Large scatter in Baldwin diagrams makes this an imprecise effect (Gaskell, 1985; Steidal and Sargent, 1991; Boroson and Green, 1992).

4 BROAD-LINE PROFILES IN SEYFERT I GALAXIES

We are able to extend the QSO disc model to cover Seyfert I broad emission-line spectra and prove that they are closely related. It will be necessary to increase either disc thickness z or density ρ_v with increasing radius. Therefore we shall arbitrarily keep ρ_v constant and increase z with increasing radius to $1 + B(r/100r_1)$ times the original value used for QSOs. Here B has to be selected for each spectrum, and $100r_1$ is a characteristic radius. Figure 7 illustrates schematic cross-sections for three Seyfert I galaxies with such proposed fanned-out discs; the values of B are given in Table II. Real disc thicknesses are unknown, relative to the radius. Had we chosen to reduce ρ_v with increasing radius, then the required fan-out would have been correspondingly greater. The effect of fan-out is to increase the line profile central peak relative to the wings.

Absorption of incident excitation flux in the disc needs to be included explicitly for normal Seyfert I profiles. Given the disc of Section 3.1.1, the incremental incident flux df absorbed by the material annulus of incremental width dr would be proportional to incident flux f and mass density:

$$\mathrm{d}f \propto -f\rho_v\,\mathrm{d}r. \tag{9a}$$

For constant density,

$$\frac{\mathrm{d}f}{f} = -\frac{\mathrm{d}r}{a}, \tag{9b}$$

where a is a characteristic radius for absorption. Integration yields the excitation flux at r:

$$f(r) = f_0 \exp\left(-\frac{r}{a}\right). \tag{9c}$$

We shall put $a = 100r_1/A$, and then A has to be selected for each line profile. Generally, values of A are chosen to accommodate the same disc thickness factor B for the Hα and Hβ profiles. For example, when the disc diameter is effectively greater for Hα than for Hβ, then A is less for Hα than for Hβ.

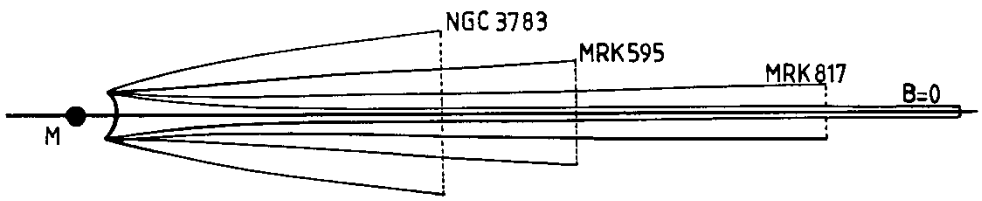

FIGURE 7 Schematic cross-sections for three Seyfert galaxies with fanned-out discs, as described in Table II. A QSO disc is also shown for comparison.

TABLE II Seyfert Broad Emission Lines.

Object	*Ion*	*z*	*FWHM* ($km\ s^{-1}$)	v_1 ($km\ s^{-1}$)	v_2 ($km\ s^{-1}$)	r_2/r_1	*A*	*B*	*Reference*	*Figure*
MRK 79	Hα	—	3585	8700	1965	20	0.9	50	Osterbrock and Shuder (1982)	8(a)
MRK 79	Hβ	—	4505	8700	2455	13	0.9	50	Osterbrock and Shuder (1982)	8(a)
MRK 335	Hα	0.025	1335	4780	285	280	0	1	Osterbrock and Shuder (1982)	8(a)
MRK 335	Hβ	0.025	1840	4780	595	64	0	1	Osterbrock and Shuder (1982)	8(a)
MRK 374	Hα	—	2760	7300	1115	43	0.8	3	Osterbrock and Shuder (1982)	8(a)
MRK 374	Hβ	—	4140	7300	1870	15	3.0	3	Osterbrock and Shuder (1982)	8(a)
MRK 486	Hα	—	1840	5600	735	58	3.0	25	Osterbrock and Shuder (1982)	8(a)
MRK 486	Hβ	—	1565	5600	735	58	1.5	25	Osterbrock and Shuder (1982)	8(a)
MRK 771	Hα	—	3400	8400	1770	22	0.3	50	Osterbrock and Shuder (1982)	8(b)
MRK 771	Hβ	—	3680	8400	2010	18	0.3	50	Osterbrock and Shuder (1982)	8(b)
MRK 817	Hα	—	3680	9700	1745	31	0.6	30	Osterbrock and Shuder (1982)	8(b)
MRK 817	Hβ	—	3860	9700	1910	26	0.6	30	Osterbrock and Shuder (1982)	8(b)
MRK 926	Hα	—	6435	12 900	2785	21	1.0	3	Osterbrock and Shuder (1982)	8(b)
MRK 926	Hβ	—	6435	12 900	2785	21	1.0	3	Osterbrock and Shuder (1982)	8(b)
III ZW 77	Hα	—	645	5050	100	2500	0.3	3	Osterbrock and Shuder (1982)	8(b)
III ZW 77	Hβ	—	825	5050	100	2500	0.6	3	Osterbrock and Shuder (1982)	8(b)
MKN 595	Hα	0.0277	2235	5265	1185	20	2.0	80	Stirpe (1990)	8(c)
MKN 595	Hβ	0.0277	2370	5265	1255	18	2.0	80	Stirpe (1990)	8(c)
MKN 1383	Hα	0.0865	5265	10 790	2535	18	0.3	3	Stirpe (1990)	8(c)
MKN 1383	Hβ	0.0865	5920	10 790	2600	17	1.0	3	Stirpe (1990)	8(c)
ESO 141-G 55	Hα	0.0370	3025	9880	1660	35	0.5	35	Stirpe (1990)	8(c)
ESO 141-G 55	Hβ	0.0370	3685	9880	1875	28	1.0	35	Stirpe (1990)	8(c)
NGC 3783	Hα	0.0096	2600	5840	1535	14.5	2.0	600	Stirpe (1990)	8(c)
NGC 3783	Hβ	0.0096	2600	5840	1535	14.5	2.0	600	Stirpe (1990)	8(c)
MKN 896	Hα	0.0263	930	4650	475	96	1.0	100	Stirpe (1990)	8(d)
MKN 896	Hβ	0.0263	1255	4650	630	55	2.0	100	Stirpe (1990)	8(d)
AKN 564	Hα	0.0244	640	4600	305	230	0.5	20	Stirpe (1990)	8(d)
AKN 564	Hβ	0.0244	735	4600	305	230	0.6	20	Stirpe (1990)	8(d)
MRK 304	Hβ	0.0659	4200	7880	2365	11.1	0.5	30	De Robertis (1985)	8(e)
MRK 335P	Hβ	0.0261	1750	5260	710	55	0.2	5	De Robertis (1985)	8(e)
MRK 841	Hβ	0.0368	4030	7880	1655	23	1.0	1	De Robertis (1985)	8(e)
I ZW 1	Hβ	0.0609	1050	6160	370	280	0	1	De Robertis (1985)	8(e)
III ZW 2	Hβ	0.0898	4510	7000	2275	9.5	1.0	3	De Robertis (1985)	8(e)
II ZW 136	Hβ	0.0632	1840	6120	770	63	1.0	7	De Robertis (1985)	8(e)

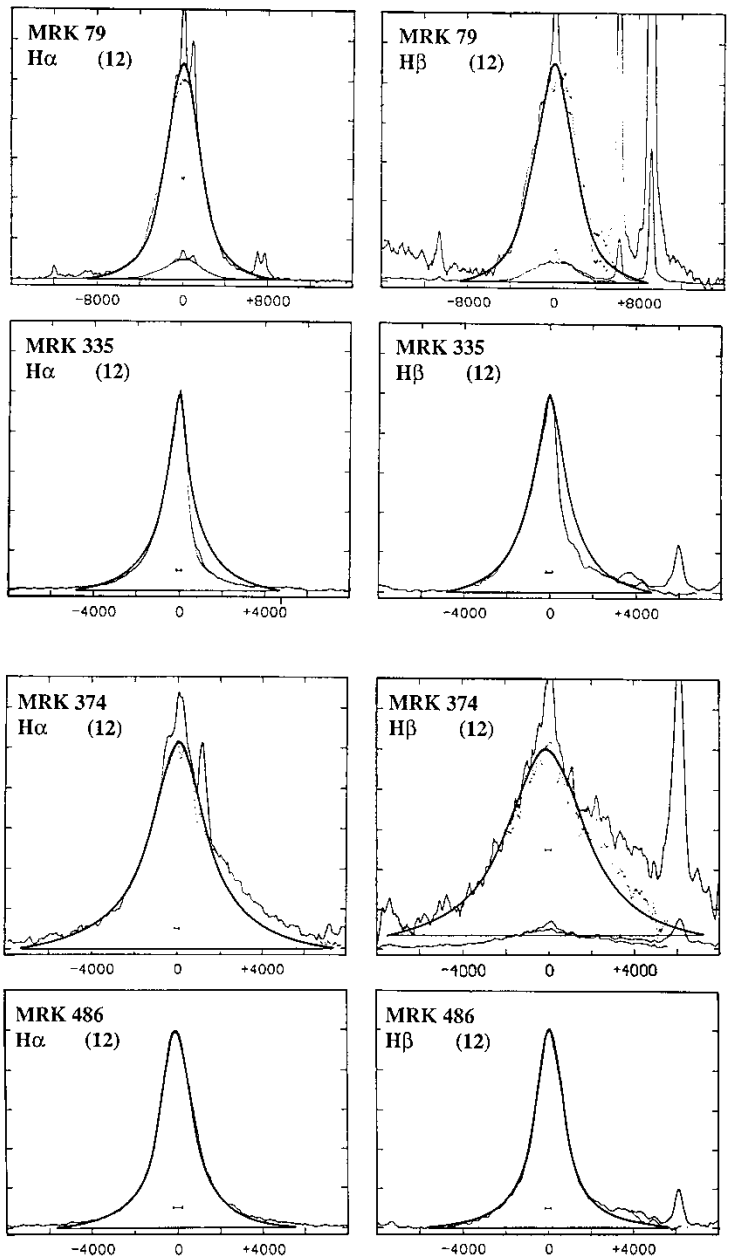

FIGURE 8 (a)–(e) Calculated Seyfert emission-line profiles fitted to various observed profiles taken from the literature, as listed in Table II, where the relevant references will be found.

Equation (5b) has therefore become more complicated for Seyfert I broad emission lines:

$$I_{\mathrm{d}u} = \int_{\varphi_2}^{\varphi_1} \exp\left(e \sin^2 \varphi\right)\left[\exp\left[-A\left(\frac{v_1}{10u}\right)^2 \cos^2 \varphi\right]\right]\left[1 + B\left(\frac{v_1}{10u}\right)^2 \cos^2 \varphi\right] . \frac{\mathrm{d}\varphi}{\cos \varphi} . \qquad (10)$$

Figure 8 illustrates a number of these theoretical profiles fitted to spectra, and Table II lists their characteristic parameters. As for QSOs, the discs vary in extent from $r_2/r_1 = 10$ up to

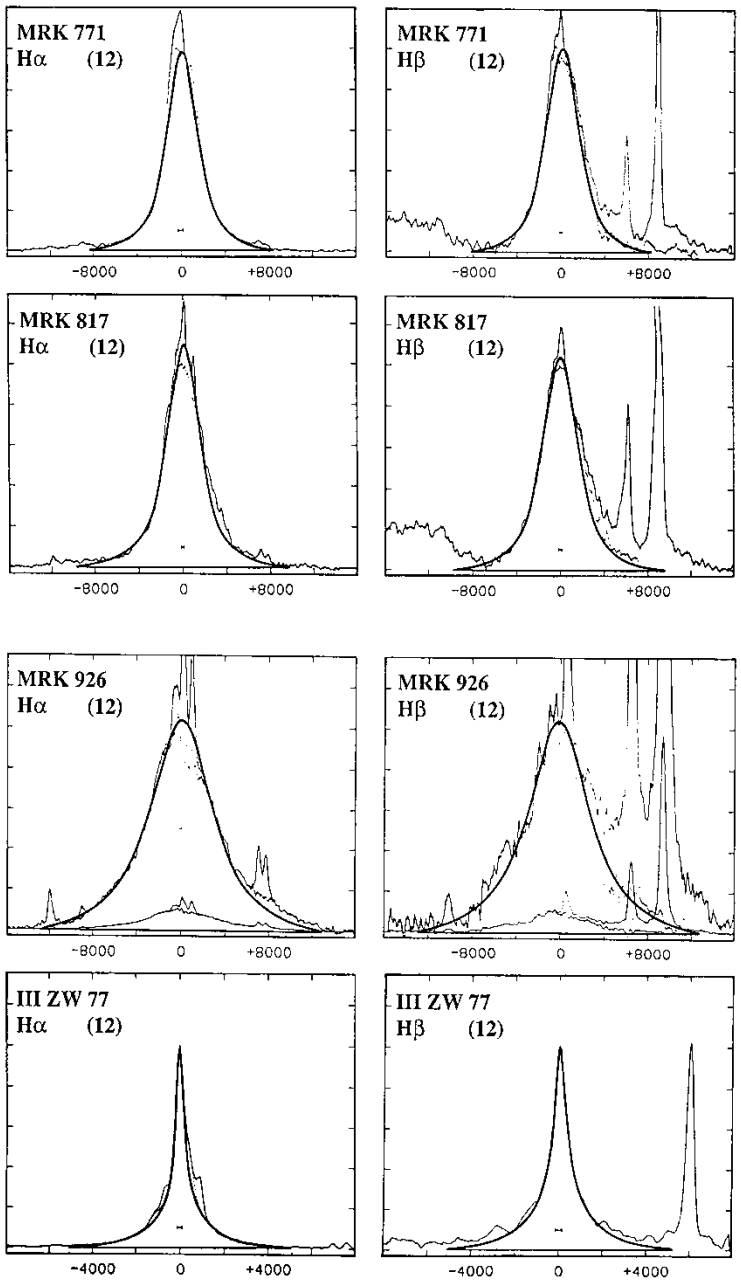

FIGURE 8b (*Continued*)

$r_2/r_1 = 2500$. The maximum rotation velocities v_1 and FWHM velocities are also similar to those found in QSOs. Consequently, QSO discs may be regarded as settled, thin Seyfert I discs.

Line broadening due to the instrumental profile has been ignored here but ideally this profile should be convolved with the complete profile from Eq. (10) before fitting to spectra (Blades *et al.*, 1980).

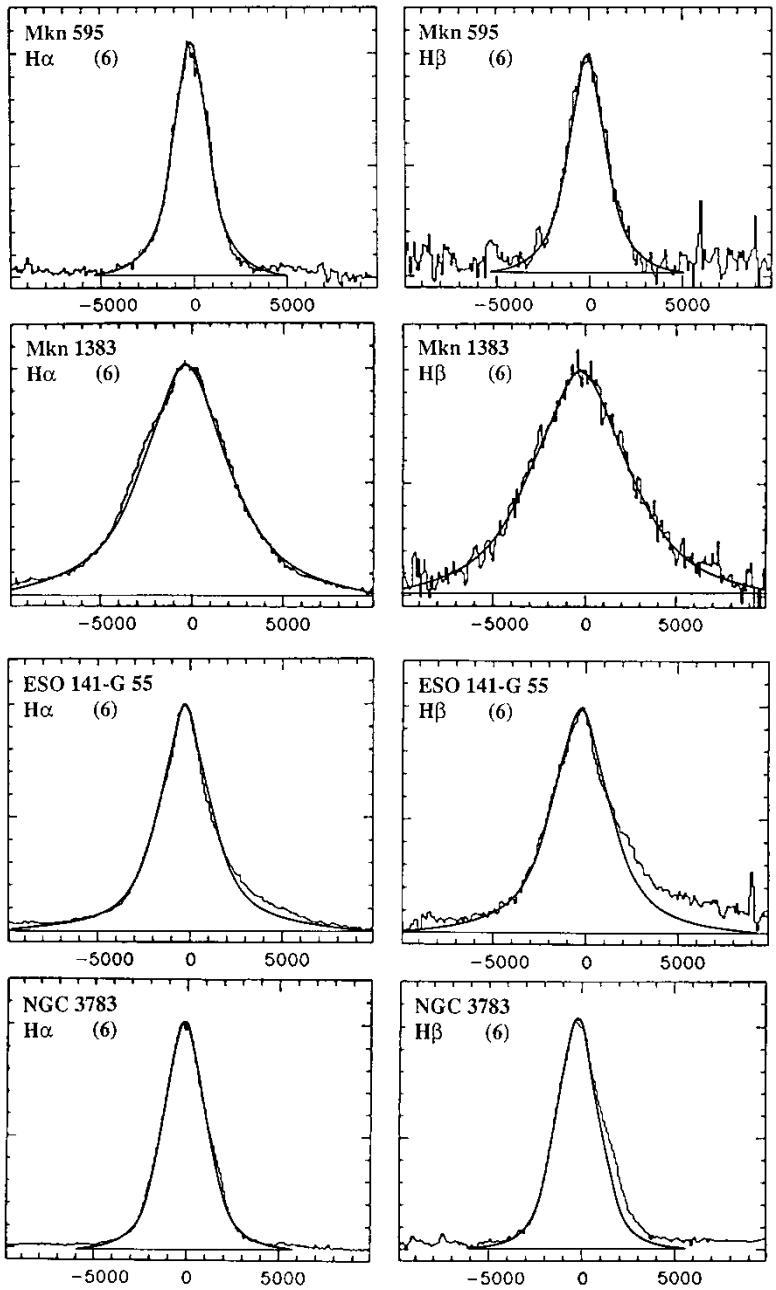

FIGURE 8c (*Continued*)

Symmetrical line profiles have been chosen plus a few with an obvious shoulder or depression. A shoulder may be produced on one side simply by increasing the illumination or mass in part of a disc, for example MRK 374. Conversely, a depression would follow from reduced illumination due to source obscuration, or less laser action in turbulent material on one side,

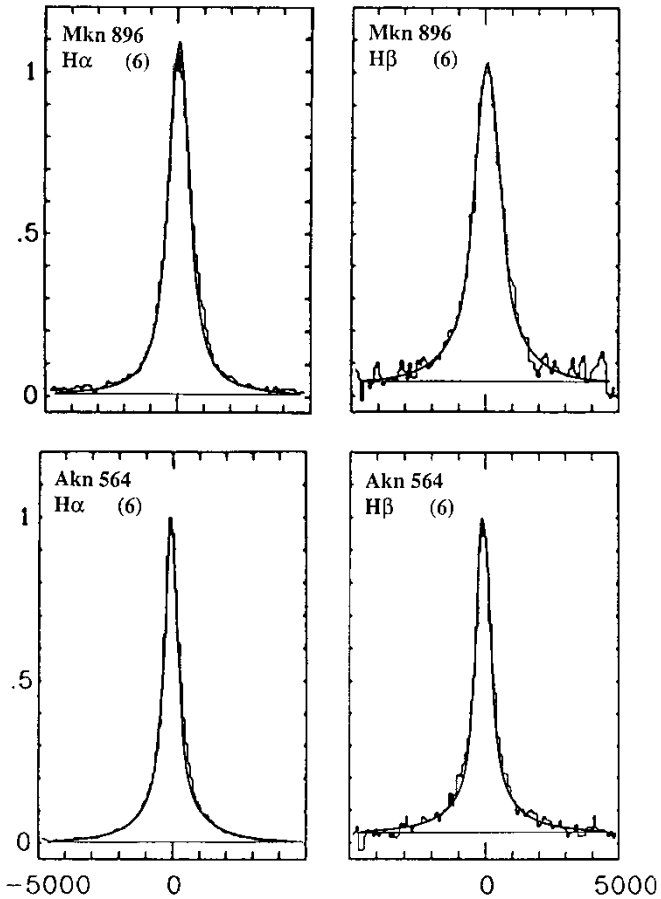

FIGURE 8e (*Continued*)

for example MRK 335. Such profiles would be expected to vary over a few years, as the disc rotates.

Spectra which appear like a narrow profile superimposed on top of a broader profile, but displaced slightly in wavelength, may sometimes be explained by Figure 9. Here, using Eq. (5b) with $r_2/r_1 = 100$, the theoretical profile on the red wing represents a disc with some darker material (due to turbulence, say) for r/r_1 values between 16 and 32. The blue wing is due to material emitting normally. The observed profile peak would probably be smooth and skewed, as suggested by the dashed curve. Unfortunately, the foot of the red wing may be interpreted as a shoulder if the line centre is fitted to the peak. In addition, the narrower profile would then fit $r_2/r_1 = 125$.

Any involvement of a narrow-line region (NLR) in the outer disc could greatly complicate the profile analysis, for example MRK 79 and others. Radial motion of disc material, gas jets and winds or absorption by dust may add asymmetries to line profiles, as demonstrated by Van Groningen (1983).

Table II reveals how Hβ emission-line profiles often come from a smaller disc extent than Hα profiles do, as if there is a definite ionization front limiting the Hβ region, but both profiles appear to have the same full width at zero intensity (Osterbrock and Shuder, 1982). So the Hβ region must coincide with the inner part of the Hα region.

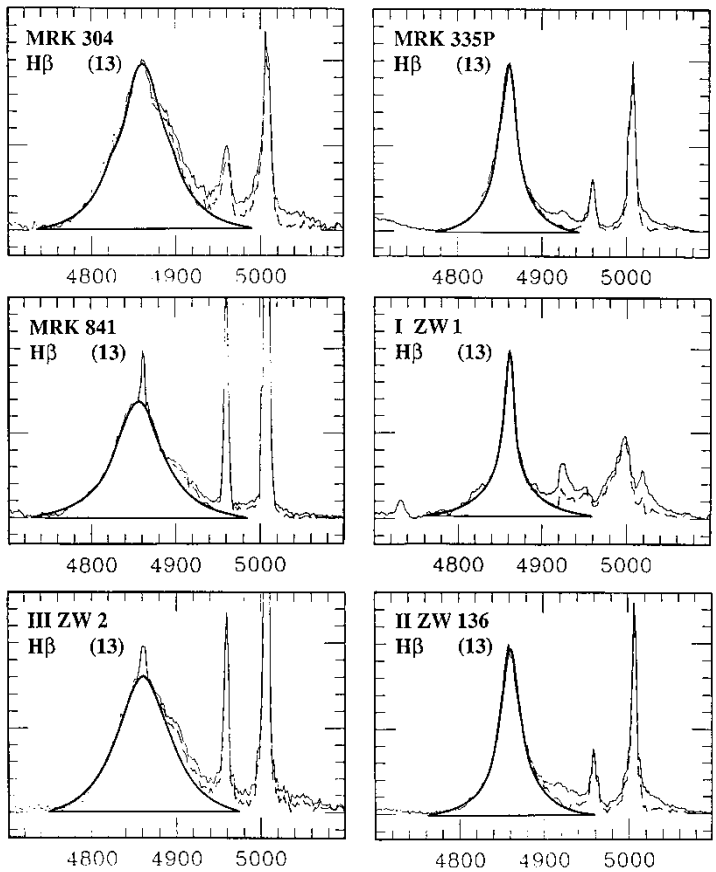

FIGURE 8e (*continued*)

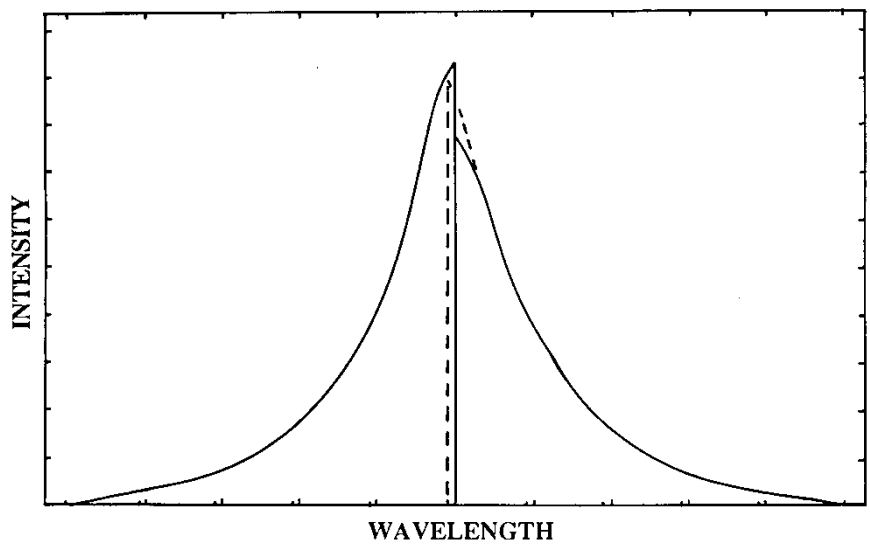

FIGURE 9 Illustration of a skewed emission-line profile produced by arbitrarily restricting emission from part of the red-wing receding material. ——, idealized real blue and red wings; – – –, a more probable smoothed distorted profile with its blue-shifted centroid.

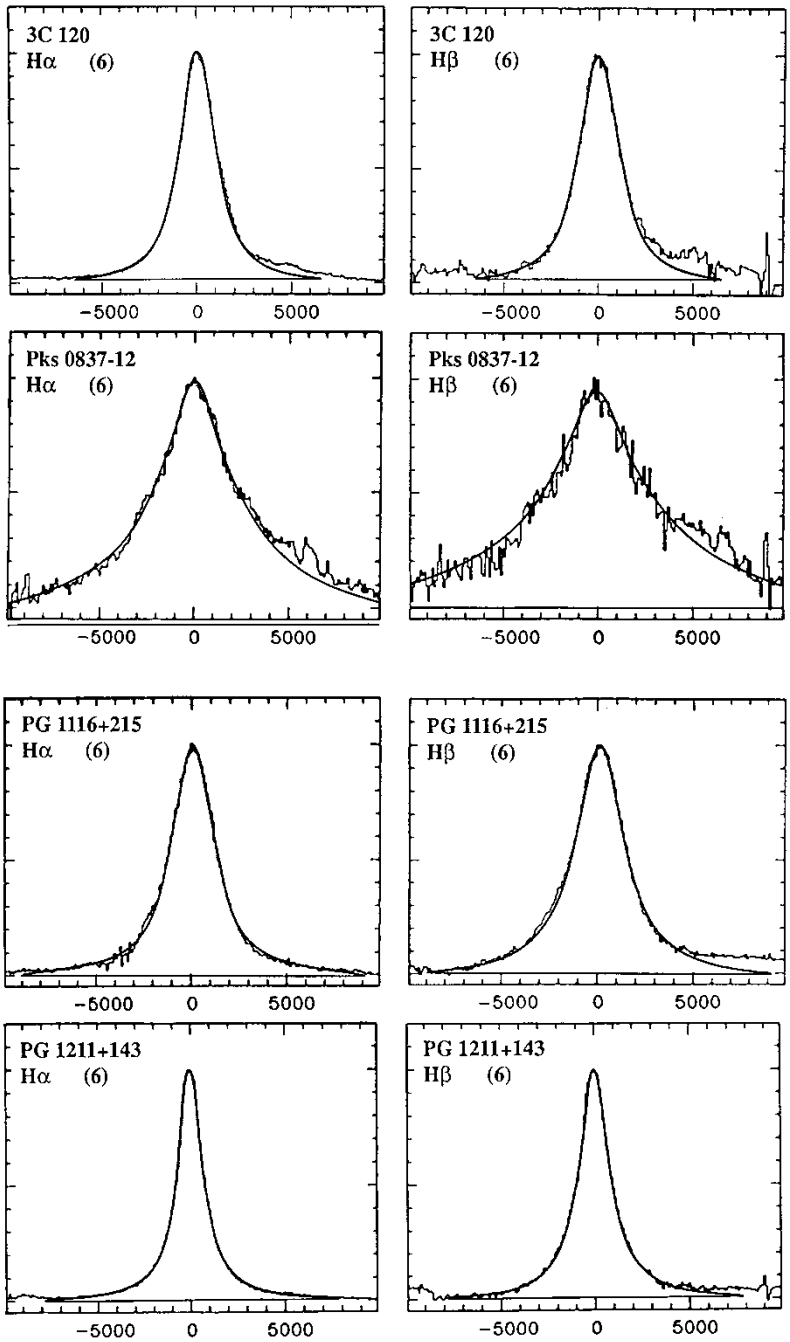

FIGURE 10 (a)–(e) Emission-line profiles calculated from Eq. (10), fitted to various observed profiles which do not fit the normal QSO–Seyfert classification, as listed in Table III, where the relevant references will be found. A composite C IV set of spectra which result simply from the effect of increasing the disc width from $r_2/r_1 = 10$ to $r_2/r_1 = 160$, while $A = 0$ and $B = 4$ remain fixed is shown in (e). The fits to IC 4329 and NGC 7469 are better than published.

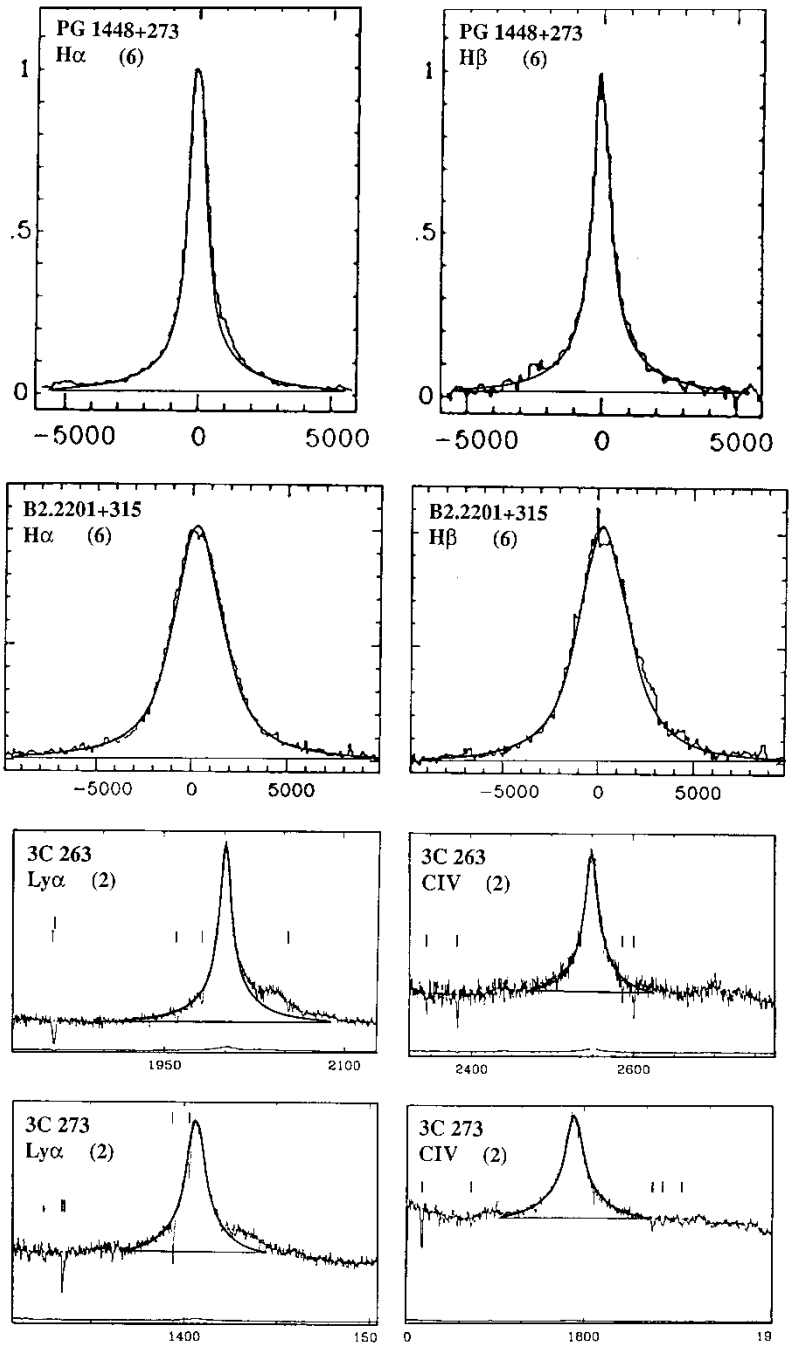

FIGURE 10b (*Continued*)

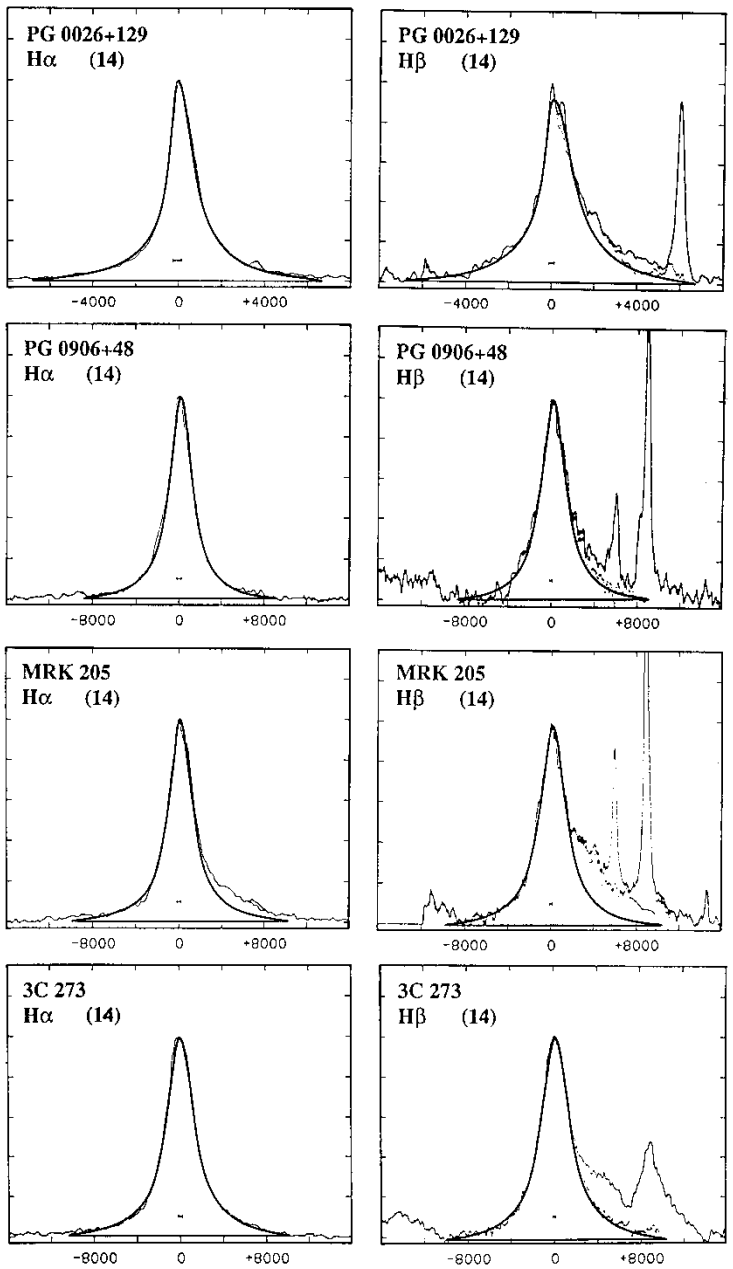

FIGURE 10c (*Continued*)

The total observed flux I_{TS} contained within an emission-line profile is no longer given by the QSO Eq. (6). For larger values of A, B and r_2/r_1, such as in MRN 896, the partial integration process now yields

$$I_{\mathrm{TSy}} \approx \text{constant} \times \int_{r_1}^{r_2} \exp(-kr) r^{-1/2}\, \mathrm{d}r. \tag{11}$$

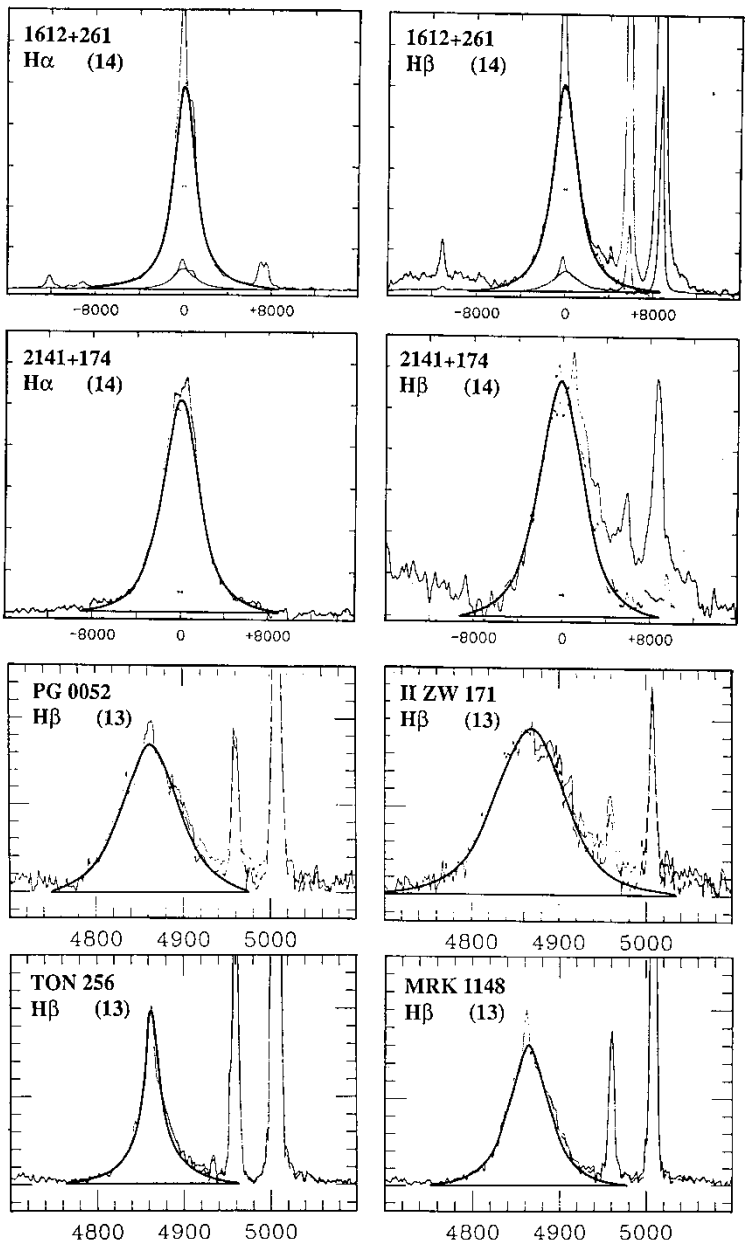

FIGURE 10d (*Continued*)

By substituting $x = r^{1/2}$, this reduces to an error function. The corresponding emission-line profile approaches a Gaussian form.

De Robertis and Osterbrock (1984) analysed some narrow-line profiles in high-ionization Seyfert I galaxies and discovered that a similar mechanism or geometry for line production must be acting in both the BLRs and NLRs of Seyfert Is and QSOs. Osterbrock and Shuder

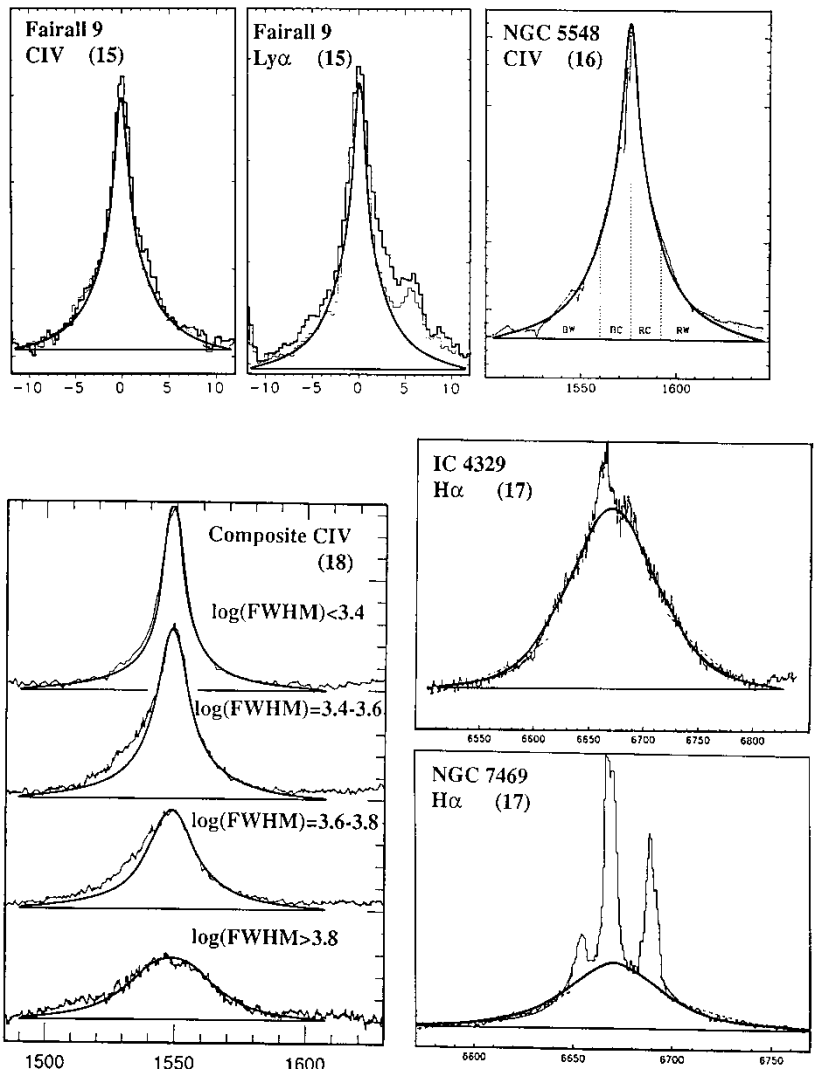

FIGURE 10e (*Continued*)

(1982) concluded that radial outflow models are not applicable and that BLR disc orientation is probably random in host galaxies.

5 BROAD-LINE PROFILES FOR VARIANTS

The straight QSO and Seyfert I classifications cover many AGNs, but some QSO profiles look like Seyfert I profiles, and vice versa. This implies that these objects occupy a continuous sequence. Figure 10 illustrates several such profiles and Table III lists the corresponding parameters. Objects with $A = B = 0$ are those Seyfert I galaxies that look like QSOs, whereas the others are QSOs obeying Eq. (10).

TABLE III Variant Broad Emission Lines.

Object	*Ion*	*z*	*FWHM* (km s^{-1})	v_1 (km s^{-1})	v_2 (km s^{-1})	r_2/r_1	*A*	*B*	*Reference*	*Figure*
3C 120	Hα	0.0330	2275	6495	1150	32	2.0	50	Stirpe (1990)	10(a)
3C 120	Hβ	0.0330	2600	6495	1310	24.5	2.0	50	Stirpe (1990)	10(a)
PKS 0837-12	Hα	0.1974	5065	16 000	320	2500	0.9	2	Stirpe (1990)	10(a)
PKS 0837-12	Hβ	0.1974	5895	16 000	320	2500	1.4	2	Stirpe (1990)	10(a)
PG 1116+215	Hα	0.1764	2765	9220	1310	50	0.5	17	Stirpe (1990)	10(a)
PG 1116+215	Hβ	0.1764	3160	9220	1320	49	2.0	17	Stirpe (1990)	10(a)
PG 1211+143	Hα	0.0813	1530	7790	820	91	0.5	25	Stirpe (1990)	10(a)
PG 1211+143	Hβ	0.0813	1945	7790	935	69	1.0	25	Stirpe (1990)	10(a)
PG 1448+273	Hα	0.0648	885	5600	335	280	0.5	10	Stirpe (1990)	10(b)
PG 1448+273	Hβ	0.0648	935	5600	335	280	0.6	10	Stirpe (1990)	10(b)
B2.2201+315	Hα	0.2959	3050	9750	1550	40	2.0	80	Stirpe (1990)	10(b)
B2.2201+315	Hβ	0.2959	3115	9750	1610	37	2.0	80	Stirpe (1990)	10(b)
3C 263	Lyα	0.652	2075	13 080	785	280	0.4	4	Bahcall *et al.* (1993)	10(b)
3C 263	C IV	0.652	2740	8860	710	156	2.0	4	Bahcall *et al.* (1993)	10(b)
3C 273	Lyα	0.158	2945	8150	815	100	0	0	Bahcall *et al.* (1993)	10(b)
3C 273	C IV	0.158	3275	10 100	1010	100	0	0	Bahcall *et al.* (1993)	10(b)
PG 0026+129	Hα	—	1450	6670	735	83	0.5	7	Shuder (1984)	10(c)
PG 0026+129	Hβ	—	1780	6670	1000	44	0.5	7	Shuder (1984)	10(c)
PG 0906+48	Hα	—	2480	9000	1215	55	0.5	18	Shuder (1984)	10(c)
PG 0906+48	Hβ	—	2815	9000	1305	48	1.0	18	Shuder (1984)	10(c)
MRK 205	Hα	—	2665	10 000	1300	59	0.5	15	Shuder (1984)	10(c)
MRK 205	Hβ	—	2890	10 000	1350	55	0.5	15	Shuder (1984)	10(c)
3C 273	Hα	0.158	3000	10 220	1430	51	0.5	10	Shuder (1984)	10(c)
3C 273	Hβ	0.158	3110	10 220	1490	47	0.5	10	Shuder (1984)	10(c)
1612+261	Hα	—	2330	8555	1155	55	0.4	25	Shuder (1984)	10(d)
1612+261	Hβ	—	2665	8555	1285	44	0.4	25	Shuder (1984)	10(d)
2141+174	Hα	—	3775	8895	2055	18.7	0.2	50	Shuder (1984)	10(d)
2141+174	Hβ	—	4620	8895	2580	11.9	0.5	50	Shuder (1984)	10(d)

TABLE III (*Continued*)

Object	*Ion*	*z*	*FWHM* ($km\ s^{-1}$)	v_1 ($km\ s^{-1}$)	v_2 ($km\ s^{-1}$)	r_2/r_1	*A*	*B*	*Reference*	*Figure*
PG 0052	Hβ	0.1544	4555	7000	2450	8.2	1.0	5	De Robertis (1985)	10(d)
II ZW 171	Hβ	0.0699	5710	10 505	3330	10.0	0.5	100	De Robertis (1985)	10(d)
TON 256	Hβ	0.1311	1490	6130	490	156	1.0	6	De Robertis (1985)	10(d)
MRK 1148	Hβ	0.0645	3330	7000	1750	16	1.2	50	De Robertis (1985)	10(d)
Fairall 9	Lyα	0.046	2550	11 750	470	625	0	0	Rodriguez-Pascual *et al.* (1997)	10(e)
Fairall 9	C IV	0.046	2755	11 750	575	415	0	0	Rodriguez-Pascual *et al.* (1997)	10(e)
NGC 5548	C IV	0.017	3440	13 510	770	310	0	0	Korista *et al.* (1995)	10(e)
Composite with log(FWHM) < 3.4	C IV	—	2345	11 445	905	160	0	4	Wills *et al.* (1993)	10(e)
Composite with log(FWHM) = 3.4–3.6	C IV	—	3115	11 445	1280	80	0	4	Wills *et al.* (1993)	10(e)
Composite with log(FWHM) = 3.6–3.8	C IV	—	4305	11 445	1810	40	0	4	Wills *et al.* (1993)	10(e)
Composite with log(FWHM) > 3.8	C IV	—	6775	11 445	3620	10	0	4	Wills *et al.* (1993)	10(e)
IC 4329	Hα	0.017	4375	7115	2560	7.3	0.5	40	Penston *et al.* (1990a)	10(e)
NGC 7469	Hα	0.016	2585	4495	1215	13.7	0.5	5	Penston *et al.* (1990a)	10(e)

6 CONCLUSIONS

A BLR disc model has been produced and fitted accurately to a large number of observed broad emission-line profiles from QSOs and Seyfert I galaxies. Low turbulence plus stimulated non-isotropic emission are key features of the model. These radical concepts make this model unique in fitting a wide range of disc sizes from $r_2/r_1 = 10$ to $r_2/r_1 = 2500$.

Results from the model include the following

(i) The QSO disc mass is proportional to (radius)$^{3/2}$.
(ii) The emission-line profile peak intensity is proportional to log(maximum radius).
(iii) The average disc rotation velocity for QSOs is around 2200 km s^{-1}.
(iv) A QSO disc contributes most of its emission-line flux from its innermost region, whereas its outer regions govern the line profile's sharpness.
(v) Seyfert I BLR discs are usually thicker or fanned out compared with the tapered QSO discs.
(vi) Some QSO line profiles look like Seyfert I line profiles, implying similar disc structures.

Acknowledgement

I would like to thank Imperial College Library staff, plus A. Rutledge for typing and R. Glovnea for computing assistance.

References

Bahcall, J. N., Bergerson, J., Boksenberg, A., Hartig, G. F., Jannuzi, B. T., Kirhakos, S. *et al.* (1993) *Astrophys. J., Suppl. Ser.* **87**, 1.
Baldwin, J. A. (1977) *Astrophys. J.* **214**, 679.
Baldwin, J. A., Burke, W. L., Gaskell, C. M. and Wampler, E. J. (1978) *Nature* **273**, 431.
Baldwin, J. A., McMahon, R., Hazard, C. and Williams, R. E. (1988) *Astrophys. J.* **327**, 103.
Baldwin, J. A., Ferland, G., Korista, K. and Verner, D. (1995) *Astrophys. J.* **455**, L119.
Beck, R. (1982) *Astron. Astrophys.* **106**, 121.
Blades, J. C., Wynne-Jones, I. and Wayte, R. (1980) *Mon. Not. R. Astron. Soc.* **193**, 849.
Boroson, T. A. and Green, R. F. (1992) *Astrophys. J., Suppl. Ser.* **80**, 109.
Brotherton, M. S., Wills, B. J., Steidel, C. C. and Sargent, W. L. W. (1994) *Astrophys. J.* **423**, 131.
Corbin, M. R. (1995) *Astrophys. J.* **447**, 496.
De Robertis, M. (1985) *Astrophys. J.* **289**, 67.
De Robertis, M. M. and Osterbrock, D. E. (1984) *Astrophys. J.* **286**, 171.
Dumont, A. M., Collin-Souffrin, S. and Nazarova, L. (1998) *Astron. Astrophys.* **331**, 11.
Foltz, C. B., Weymann, R. J., Peterson, B. M., Sun, L., Malkan, M. A. and Chattes, F. H. (1986) *Astrophys. J.* **307**, 504.
Gaskell, C. M. (1985) *Astrophys. J.* **291**, 112.
Glazier, E. V. D. and Lamont, H. R. L. (1958) *The Services Textbook of Radio*, Vol. 5, *Transmission and Propagation*. HMSO, London.
Haas, M., Lemke, D., Stickel, M., Hippelein, H., Kunkel, M., Herbstmeier, U. and Maltila, K. (1998) *Astron. Astrophys.* **338**, L33.
Jackson, N. and Eracleous, M. (1995) *Mon. Not. R. Astron. Soc.* **276**, 1409.
Kinney, A. L., Rivolo, A. R. and Koratkar, A. P. (1990) *Astrophys. J.* **357**, 338.
Korista, K. T., Alloin, D., Barr, P., Clavel, J., Cohen, R. D., Crenshaw, D. M. *et al.* (1995) *Astrophys. J., Suppl. Ser.* **97**, 285.
Osterbrock, D. E. (1989) *Astrophysics of Gaseous Nebulae and Active Galactic Nuclei*. University Science Books, California.
Osterbrock, D. E. (1991) *Rep. Prog. Phys.* **54**, 579.
Osterbrock, D. E. and Shuder, J. M. (1982) *Astrophys. J., Suppl. Ser.* **49**, 149.
Penston, M. V., Croft, S., Basu, D. and Fuller, N. (1990a) *Mon. Not. R. Astron. Soc.* **244**, 357.
Penston, M. V., Robinson, A., Alloin, D., Appenzeller, I., Aretxaga, I., Axon, D. J. *et al.* (1990b) *Astron. Astrophys.* **236**, 53.
Rodriguez-Pascual, P. M., Alloin, D., Clavel, J., Crenshaw, D. M., Horne, K., Kruss, G. A. *et al.* (1997) *Astrophys. J., Suppl. Ser.* **110**, 9.
Sargent, W. L. W., Boksenberg, A. and Steidel, C. C. (1988) *Astrophys. J., Suppl. Ser.* **68**, 539.

Sargent, W. L. W., Steidel, C. C. and Boksenberg, A. (1989) *Astrophys. J., Suppl. Ser.* **69**, 703.
Shuder, J. M. (1984) *Astrophys. J.* **280**, 491.
Sokolnikoff, I. S. and Redheffer, R. M. (1958) *Mathematics of Physics and Modern Engineering*. McGraw-Hill, New York.
Steidel, C. C. and Sargent, W. L. W. (1991) *Astrophys. J.* **382**, 433.
Steidel, C. C. and Sargent, W. L. W. (1992) *Astrophys. J., Suppl. Ser.* **80**, 1.
Stirpe, G. M. (1990) *Astron. Astrophys., Suppl. Ser.* **85**, 1049.
Van Groningen, E. (1983) *Astron. Astrophys.* **126**, 363.
Wills, B. J. *et al.* (1993) *Astrophys. J.* **415**, 563.
Young, P., Sargent, W. L. W. and Boksenberg, A. (1982) *Astrophys. J., Suppl. Ser.* **48**, 455.

APPENDIX A

We need an equilibrium BLR disc photon field to account for universal profiles. The empirical equation (4b) is thought to be based on laser amplification, subject to Poisson's law of probability (Sokolnikoff and Redheffer, 1958, p. 655):

$$B(s) \approx \left(\frac{\mu^{\mathbf{s}}}{s!}\right) \exp(-\mu). \tag{A1}$$

We can only view the output from the BLR disc rather than the internal processes. Therefore, it is proposed that μ stands for the average number of stimulated line-photons produced in the BLR disc by any given final output photon. The actual number is s, which is usually different from μ. So $B(s)$ is the partial random probability that s stimulated photons have been produced directly by any given final photon. The sum of all the partial probabilities is unity: $\sum B(s) = 1$. If for example $\mu = 1$, then e^{-1} is the probability that a given final photon stimulated one other photon. This is also equal to the probability that it stimulated none. It follows that the probability of two or more stimulated emissions per final photon is significant, at 26%.

Since many of these stimulated photons have stimulated others, we are interested in $sB(s)$, summed and normalized. An added complication involves the strong dependence of both stimulated and spontaneous emission on $\sin^2 \varphi$. Therefore, if E is the instantaneous line-photon emission travelling in direction φ towards us through the disc, the partial increase ΔE due to a stimulation partial probability $B(s)$ is

$$\Delta E = E \sin^2 \varphi \frac{sB(s)}{\mu B(\mu)}. \tag{A2}$$

This needs to be summed over all integral values of s. Now, $s/s!$ is well behaved, even for non-integral values of s (Sokolnikoff and Redheffer, 1958, p. 163). So equation (A2) with the introduction of equation (A1) may be written

$$\int_{E_0}^{E_m} \frac{dE}{E} = \text{constant} \approx \frac{\sin^2 \varphi}{\mu B(\mu)} \sum_{s=0}^{\infty} \frac{s}{s!} (\mu^s \exp(-\mu). \tag{A3}$$

Integration of the left-hand side and summation of the right-hand side produce the final flux from the BLR disc:

$$\begin{aligned} E_m &\approx E_0 \exp\left[\left(\frac{e}{\mu}\right)^{\mu} u! \sin^2 \varphi\right] \\ &\approx E_0 \exp(e \sin^2 \varphi), \qquad \text{for } \mu \approx 1. \end{aligned} \tag{A4}$$

To understand why $\mu = 1$ for BLR discs, consider an idealized situation in which a single spontaneous photon stimulates the emission of a photon; then these two photons go on to stimulate others until 2^n result from this repetitive doubling process. At the end, half of the photons have been created by stimulation but have not stimulated others. A quarter of the photons have stimulated one other photon, while an eighth have stimulated two other photons, and so on. So the average number of stimulations per final photon is $(2^n - 1)/2^n = \mu \approx 1$. In practice the amplification occurs randomly but, for N final photons produced from one spontaneous photon, we still have $\mu = (N-1)/N \approx 1$.

Amplification ceases when the available ions awaiting stimulation are depleted such that absorption of photons approaches emission rate. E_0 represents a mixture of stimulated plus spontaneous photons at some earlier stage of the process and increases with increasing photo-ionization source intensity.